We are IntechOpen, the world's leading publisher of Open Access books
Built by scientists, for scientists

4,800
Open access books available

122,000
International authors and editors

135M
Downloads

Our authors are among the

154
Countries delivered to

TOP 1%
most cited scientists

12.2%
Contributors from top 500 universities

CLARIVATE ANALYTICS
BOOK CITATION INDEX
INDEXED

WEB OF SCIENCE™

Selection of our books indexed in the Book Citation Index in Web of Science™ Core Collection (BKCI)

Interested in publishing with us?
Contact book.department@intechopen.com

Numbers displayed above are based on latest data collected.
For more information visit www.intechopen.com

6

To Design a Small Pneumatic Actuator Driven Parallel Link Mechanism for Shoulder Prostheses for Daily Living Use

Masashi Sekine, Kento Sugimori and Wenwei Yu
Chiba University
Japan

1. Introduction

Only in Japan, there are about 82,000 upper limb amputees (Ministry of Health, Labour and Welfare, 2005). Using upper limb prostheses could restore the function for them, thus improve significantly the quality of their activities of daily living [ADL]. Compared with below-elbow prostheses, shoulder prostheses are left behind in their development, due to high degrees of freedom [DOF] required, which demands a large number of actuators, thus denotes a large size and a heavy weight, and complicated control mechanism.

Recently, there is a certain body of research on developing robotic devices that could be used as prostheses for shoulder amputees (Jacobson et al., 1982; Motion Control, Inc., 2006-2011; The Johns Hopkins University Applied Physics Laboratory [APL], 2011; Troncossi et al., 2005, 2009a, 2009b). These research efforts have led to artificial prostheses with high functionality and performance. For example, the prosthetic arm of Defense Advanced Research Projects Agency and APL, has 25 DOFs, individual finger movements, dexterity that approaches that of the human limb, natural control, sensory feedback, and a number of small wireless devices that can be surgically implanted (or injected) to allow access to intramuscular signals(APL, 2011). The *Utah Arm 3*, a modification of the previous *Utah Arm* that has been the premier myoelectric arm for above elbow amputees, has two microcontrollers that are programmed for the hand and elbow, accordingly, allowing separate inputs and hence simultaneous control of both, and that is, the wearer can operate the hand and elbow concurrently for natural function (Jacobson et al., 1982; Motion Control, Inc., 2006-2011). The hybrid electric prosthesis for single arm amputee of Tokyo Denki University possesses a ball joint of 3 DOFs in humeral articulation. Patient operates the prosthesis to optional point by pressing a switch with the other healthy limb to free the joint, and releases to fix and hold the prosthetic arm stably (Nasu et al., 2001). Moreover, the electromechanical shoulder articulation with 2 DOFs for upper-limb prosthesis that has two actuated joints embedded harmonic drives, an inverted slider crank mechanism, and ball screw, has been developed (Troncossi et al., 2005, 2009a, 2009b).

These prostheses have the following characteristics: they are more or less anthropomorphic, basically supported by metal frames or parts, driven by electric motors, therefore, many of them seem to be not suitable for the daily living use: they are not light weight, not convenient, with a bad portability, and lack of backdrivability which could contribute to the safety use in daily living.

Using pneumatic actuators (Festo AG & Co. KG, 2002-2008; Folgheraiter & Gini, 2005), some researchers have developed sophisticated manipulators having structure similar to human upper limb. Employing pneumatic actuators that could naturally realize backdrivability, ensures safety against collisions or contact between the prosthetic shoulder and its environments around. In the *Airic's_arm* (Festo AG & Co. KG, 2000-2008), 30 artificial muscles were used to move the artificial bone structure comprising the ulna, radius, the metacarpal bones and the bones of the fingers, as well as the shoulder joint and the shoulder blade. The *MaximumOne*, a robot arm of Artificial Intelligence and Robotics Laboratory, Politecnico di Milano, consists of two joints with 4 DOFs in all. The shoulder is made up of a ball joint with 3 DOFs and driven by five actuators, and the elbow is a revolute joint with 1 DOF and driven by two actuators (Folgheraiter & Gini, 2005). However, the manipulators are basically not for prosthetic use, moreover, they are not portable, especially due to the big air compressor.

This study aims to develop a lightweight shoulder prosthesis that could be easily fitted to and carried by amputees, therefore a convenient one. This chapter presents kinematical analysis, procedure for finding optimal configurations for the prosthetic arm, and verification of the design concepts.

2. Design concepts

A shoulder prosthesis for daily living use should be light-weight, portable, and safe. Consideration to design such a shoulder prosthesis is described as follows.

1. Using small pneumatic actuators driven by small portable air compressor for weight saving and portability. To meet portability and light-weight requirements, small actuators and compressors are musts for shoulder prostheses. The pneumatic actuators Sik-t, Sik-t Power-Type (Squse Inc.: 1g, 20N; 3g, 130N), air compressors MP-2-C (Squse Inc.: 180g, 0.4 MPa) are products developed recently for robotic application with light-weight and good portability. In this research, these products were employed as actuators and their air sources. The purpose of this research is to design shoulder prostheses with optimal spatial functionality using these actuators.
2. Employing a parallel link mechanism to enable high rigidity and high torque output. The natural viscoelasticity of pneumatic actuators could contribute to backdrivability, and safety of shoulder prostheses, however, it also affects the payload of the system. Moreover, since small actuators have a limited tensile force, a structure that could exert high torque output is preferable. That is why a parallel link mechanism that could improve structural rigidity was employed. However, the parallel link structure usually has a limited stretch along axial direction. The working space of the prostheses should be adjusted to fit individual users' expected frequently accessed area [EFAA]. To the best of our knowledge, there are no investigation results reported on how to match working space of end-effector to EFAA of individual users' hand. This is the main objective of this study.
3. Using a rubber backbone for the parallel link mechanism to enable trade-off between working space and payloads. Since, the parallel link structure usually has a limited stretch along axial direction. A flexible backbone for the parallel link could give more possibility to deal with the trade-off between payloads and working space, however, this raises one more design variable, which should also be carefully investigated in the design process. This is an on-going research theme, and will be addressed in other papers.

4. Designing a special backpack that could contain the shoulder prostheses and all accessories, and could be worn by the amputee user himself with minimal effort. This needs the shoulder prosthesis be foldable, and the backpack be designed for conveniently getting the shoulder prosthesis in and out. This will be approached in the next stage and addressed in other papers. The ultimate goal of this study is to build a shoulder prosthesis that could be used in daily living by shoulder amputees. The purpose of this paper is to describe the structure of the prosthesis, and approach to find optimal configurations based on the aforementioned design consideration. Fig. 1 shows an illustration of the shoulder prosthetic system, which is drafted with computer aided design [CAD] software SolidWorks (Dassault Systèmes SolidWorks Corp.) and human body model from HumanWorks software (zetec, Ltd.)

The remainder of this chapter is organized as follows. At first, in section 3, the basic structure of the prosthesis was described and several formulae for kinematics and statics of it were derived for further analysis. After that, the way to achieve the spatial accessibility and manipulability was explained in section 4. Then several experimental results concerning the design of the prosthesis were shown with discussion. Following that, a conclusion was given based on the results and discussion.

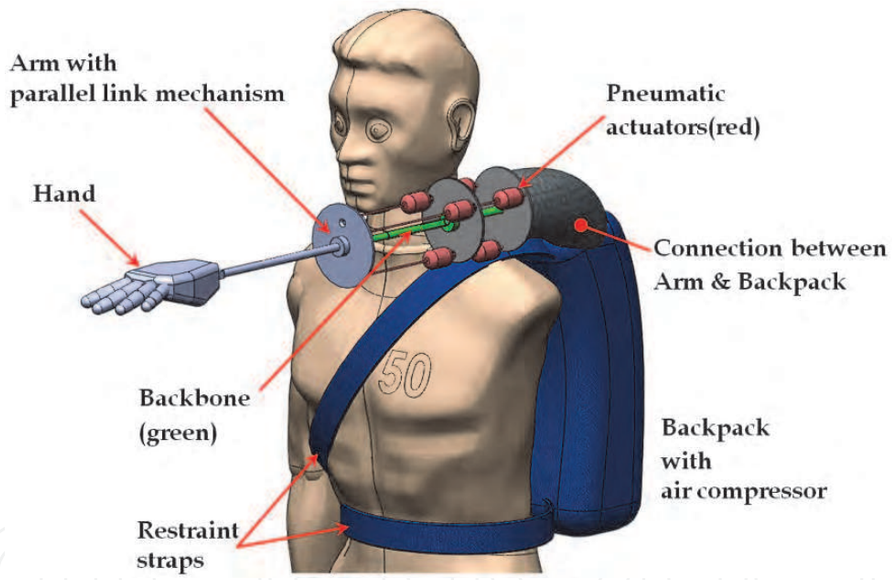

Fig. 1. The shoulder prosthetic system.

3. Kinematics and statics

To decide the physical dimension of the shoulder prosthesis, both the kinematics, statics of the prosthesis and the spatial configuration, expected frequently accessed area [EFAA] of users' hand should be considered. In this section, the kinematics and statics of the proposed shoulder prosthesis were derived for further analysis. Several estimative indexes were also defined to compare different potential solutions, thus to decide physical dimensions (configuration) of the shoulder prosthesis. As described before, only the arm structure was modelled and analyzed, whereas the prosthesis with hand, the backpack, and the connection between arm structure and backpack were left for further studies.

3.1 Arm structure

The details of the arm structure (in the following explanation, denoted as the *Arm*) are shown in Fig. 2. The *Arm* is composed of three segments. *Segment* 1 links two disks called the *Base* 1 and the *Platform* 1 with the *Backbone* 1 and three pneumatic actuators, placed equiangularly with respect to the center of the *Base* 1. The *Backbone* 1 is fixed to the center of the *Base* 1, and connected to the center of the *Platform* 1 with two passive revolute joints. To simplify the analysis, the *Backbone* 1 was assumed as a compression spring that can only move along longitudinal direction, but not as a rubber rod as described in the design concept section. By assembling *Base* 1 and *Platform* 1 with a compressed *Backbone* 1, actuators and wires that connect the pneumatic actuators with two disks are constantly loaded. This allows the *Platform* 1 to move along the longitudinal direction of the *Backbone* 1, turn around the joint of *Platform* 1 and *Backbone* 1, as a result of length changes of the three actuators.

The *Platform* 1 disk of *Segment* 1 is also used as the *Base* 2 disk of the *Segment* 2, which has a similar structure with the *Segment* 1, but with a different length. *Segment* 3 contains only a rigid rod (*Rod*) fixed to the center of outside the *Platform* 2, i.e. the *Base* 3 of the *Segment* 3. For the convenience of description, let h_1, h_2 and l_R be the initial length of the *Backbone* 1, 2 and *Rod* respectively.

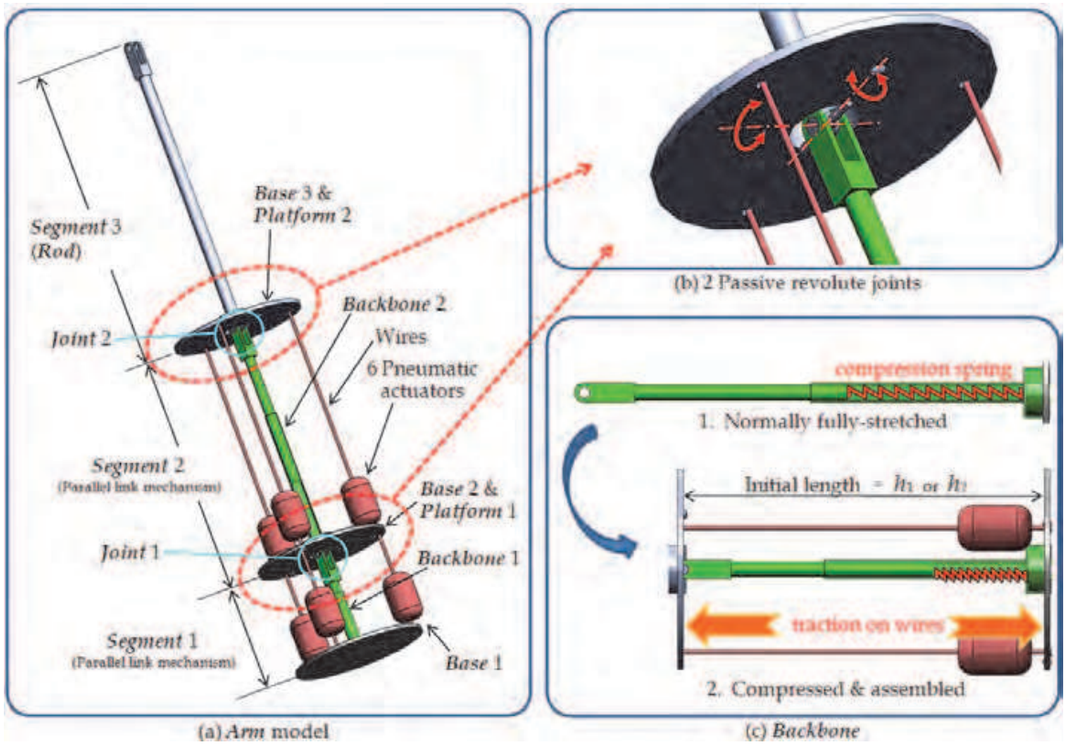

Fig. 2. The structure of the *Arm*.

3.2 Kinematics

In order to analyze the behavior of end-effector and working space of the *Arm*, forward and inverse kinematics model of the parallel link mechanism were derived.

The coordinate system of the *Arm* is shown in Fig. 3. Without loss of the generality, the thicknesses of all disks, and the shaft diameters of *Backbone* 1, 2, *Rod* were set to 0. The global

coordinate system O_{B1}-XYZ is located at the center of the *Base* 1, with the Z-axis directed along the *Backbone* 1. The contact points of three pneumatic actuators to *Base* 1 (B_{11}, B_{12}, B_{13}) were aligned equiangularly along the peripheral of a circle with a radius r_B, and B_{11} is on the X-axis.

The local coordinate system O_{P1}-$x_{P1}y_{P1}z_{P1}$ locates at the center of disk *Platform* 1, h_1 away from O_{B1} along the Z-axis. The contact points of pneumatic actuators to *Platform* 1 (P_{11}, P_{12}, P_{13}) are on radius r_P. In turn, the contact points of three pneumatic actuators to *Base* 2 (B_{21}, B_{22}, B_{23}) are equiangularly set on circumference of a circle, radius r_B, and B_{21} is on the x_{P1}-axis. The local coordinate system O_{P2}-$x_{P2}y_{P2}z_{P2}$ is set at the center of *Platform* 2, and the distance from O_{P1} is h_2. The contact points (P_{21}, P_{22}, P_{23}) are aligned equiangularly along the peripheral of a circle with a radius r_P, and P_{21} is on the x_{P2}-axis.

Finally, the *Rod* of length l_R is fixed up at O_{P2} along the z_{P2}-axis.

Suppose the actuators are activated, and their lengths change (expressed discretely: l_i gets to l_i', i =1, ..., 6). Therefore, h_1 and h_2 are converted to h_1' and h_2', two passive joints (*Joint* 1) of *Platform* 1 and the one (*Joint* 2) of *Platform* 2 rotate by α, β, γ, σ (see Fig. 2, 3), respectively.

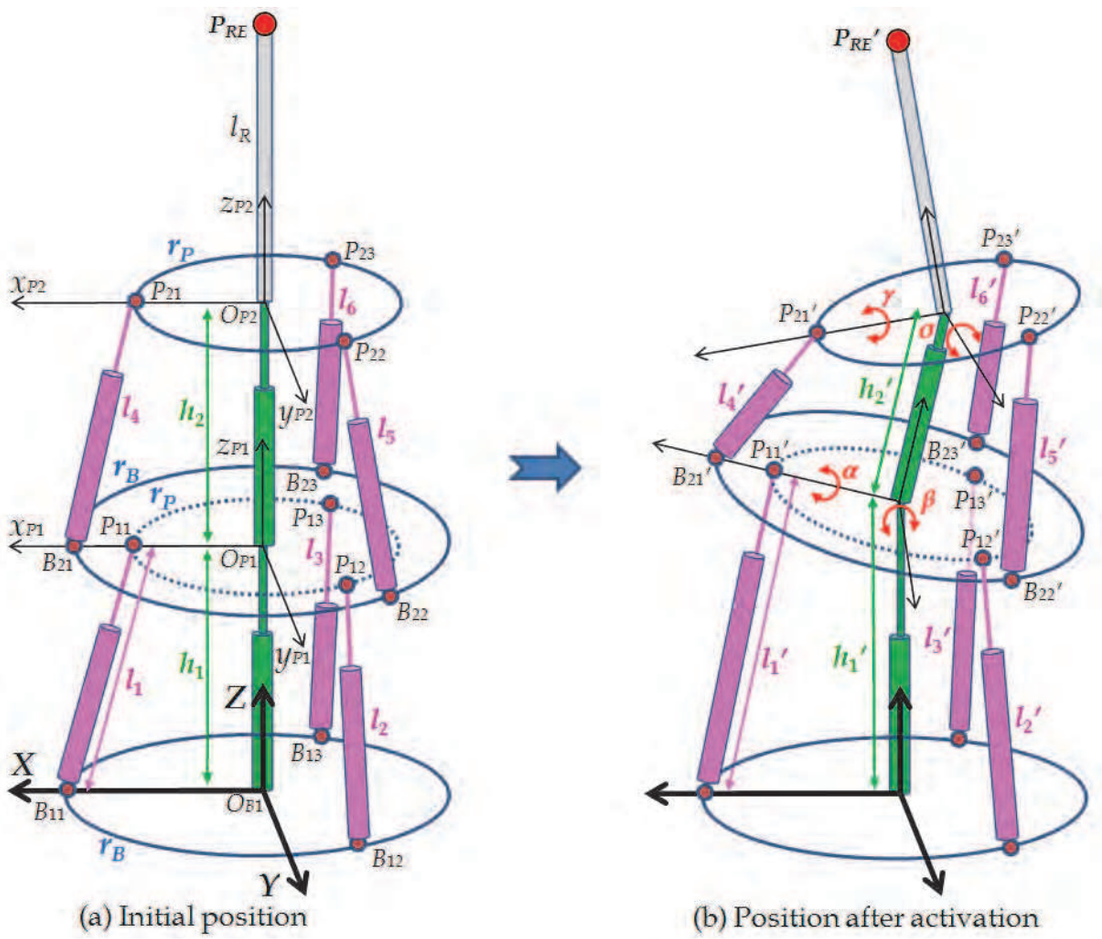

Fig. 3. Geometry of the parallel link arm.

At first, the position of O_{P1}, P_{1i}, P_{1i}'(i=1, 2, 3) and the rotation matrix $\boldsymbol{R}_1$ of *Joint* 1 in O_{P1}-$x_{P1}y_{P1}z_{P1}$, i.e. ${}^{P1}O_{P1}$, ${}^{P1}P_{1i}$, ${}^{P1}P_{1i}'$ and ${}^{P1}\boldsymbol{R}_1$ can be presented as follows:

$$ {}^{P1}\boldsymbol{O}_{P1}:(0,0,0),\quad {}^{P1}\boldsymbol{P}_{11}:(r_P,0,0),\quad {}^{P1}\boldsymbol{P}_{12}:(-\frac{1}{2}r_P,\frac{\sqrt{3}}{2}r_P,0),\quad {}^{P1}\boldsymbol{P}_{13}:(-\frac{1}{2}r_P,-\frac{\sqrt{3}}{2}r_P,0) \tag{1} $$

$$ {}^{P1}\boldsymbol{R}_1=\begin{pmatrix}1 & 0 & 0\\ 0 & cos\alpha & -sin\alpha\\ 0 & sin\alpha & cos\alpha\end{pmatrix}\begin{pmatrix}cos\beta & 0 & sin\beta\\ 0 & 1 & 0\\ -sin\beta & 0 & cos\beta\end{pmatrix}=\begin{pmatrix}cos\beta & 0 & sin\beta\\ sin\alpha sin\beta & cos\alpha & -sin\alpha cos\beta\\ -cos\alpha sin\beta & sin\alpha & cos\alpha cos\beta\end{pmatrix} \tag{2} $$

And,

$$ {}^{P1}\boldsymbol{P}_{1i}{}'={}^{P1}\boldsymbol{R}_1\,{}^{P1}\boldsymbol{P}_{1i}\quad (i=1,2,3) \tag{3} $$

Therefore, the coordinate of each element of ${}^{P1}P_{1i}'$ is:

$$ \begin{aligned} &{}^{P1}\boldsymbol{P}_{11}':(r_P cos\beta, r_P sin\alpha sin\beta, -r_P cos\alpha sin\beta)\\ &{}^{P1}\boldsymbol{P}_{12}':(-\frac{1}{2}r_P cos\beta, -\frac{1}{2}r_P sin\alpha sin\beta+\frac{\sqrt{3}}{2}r_P cos\alpha, \frac{1}{2}r_P cos\alpha sin\beta+\frac{\sqrt{3}}{2}r_P sin\alpha)\\ &{}^{P1}\boldsymbol{P}_{13}':(-\frac{1}{2}r_P cos\beta, -\frac{1}{2}r_P sin\alpha sin\beta-\frac{\sqrt{3}}{2}r_P cos\alpha, \frac{1}{2}r_P cos\alpha sin\beta-\frac{\sqrt{3}}{2}r_P sin\alpha) \end{aligned} \tag{4} $$

Next, P_{1i}', B_{1i}'in O_{B1}-XYZ, i.e. ${}^{B1}P_{1i}'$ and ${}^{B1}B_{1i}'$ can be defined as:

$$ {}^{B1}\boldsymbol{B}_{11}:(r_B,0,0),\quad {}^{B1}\boldsymbol{B}_{12}:(-\frac{1}{2}r_B,\frac{\sqrt{3}}{2}r_B,0),\quad {}^{B1}\boldsymbol{B}_{13}:(-\frac{1}{2}r_B,-\frac{\sqrt{3}}{2}r_B,0) \tag{5} $$

$$ {}^{B1}\boldsymbol{P}_{1i}{}'={}^{P1}\boldsymbol{P}_{1i}{}'+(0,0,h_1')^T\quad (i=1,2,3) \tag{6} $$

So, each element of ${}^{B1}P_{1i}'$ can be expressed as:

$$ \begin{aligned} &{}^{B1}\boldsymbol{P}_{11}':(r_P cos\beta, r_P sin\alpha sin\beta, -r_P cos\alpha sin\beta+h_1')\\ &{}^{B1}\boldsymbol{P}_{12}':(-\frac{1}{2}r_P cos\beta, -\frac{1}{2}r_P sin\alpha sin\beta+\frac{\sqrt{3}}{2}r_P cos\alpha, \frac{1}{2}r_P cos\alpha sin\beta+\frac{\sqrt{3}}{2}r_P sin\alpha+h_1')\\ &{}^{B1}\boldsymbol{P}_{13}':(-\frac{1}{2}r_P cos\beta, -\frac{1}{2}r_P sin\alpha sin\beta-\frac{\sqrt{3}}{2}r_P cos\alpha, \frac{1}{2}r_P cos\alpha sin\beta-\frac{\sqrt{3}}{2}r_P sin\alpha+h_1') \end{aligned} \tag{7} $$

Accordingly, the length of each actuator can be defined:

$$ l_i'=\overline{{}^{B1}\boldsymbol{P}_{1i}{}'{}^{B1}\boldsymbol{B}_{1i}}\quad (i=1,2,3) \tag{8} $$

By Equation (5), (7) and (8), the equations describing the relation between the lengths of pneumatic actuators, wires attached in *Segment* 1, *Backbone* 1, and the angles of two revolute joints can be defined as follows:

$$ (l_1')^2=(r_P\cos\beta-r_B)^2+(r_P\sin\alpha\sin\beta)^2+(-r_P\cos\alpha\sin\beta+h_1')^2 $$

$$
\begin{aligned}
(l_2')^2 &= \left(-\frac{1}{2}r_P\cos\beta+\frac{1}{2}r_B\right)^2 + \left(-\frac{1}{2}r_P\sin\alpha\sin\beta+\frac{\sqrt{3}}{2}r_P\cos\alpha-\frac{\sqrt{3}}{2}r_B\right)^2 \\
&\quad+\left(\frac{1}{2}r_P\cos\alpha\sin\beta+\frac{\sqrt{3}}{2}r_P\sin\alpha+h_1'\right)^2 \\
(l_3')^2 &= \left(-\frac{1}{2}r_P\cos\beta+\frac{1}{2}r_B\right)^2 + \left(-\frac{1}{2}r_P\sin\alpha\sin\beta-\frac{\sqrt{3}}{2}r_P\cos\alpha+\frac{\sqrt{3}}{2}r_B\right)^2 \\
&\quad+\left(\frac{1}{2}r_P\cos\alpha\sin\beta-\frac{\sqrt{3}}{2}r_P\sin\alpha+h_1'\right)^2
\end{aligned}
\tag{9}
$$

Equation (9) is a simultaneous equation with three unknown variables, α, β, h_1'. In the case that the lengths l_1', l_2', l_3' are given, it is possible to calculate α, β, h_1' by using the Newton method (Ku, 1999; Merlet, 1993; Press et al., 1992). Similarly, for the *Segment* 2 (i.e. in O_{P1}-$x_{P1}y_{P1}z_{P1}$), the following equation can be derived. In the case that the length l_4', l_5', l_6', are given, it is possible to calculate γ, σ, h_2'.

$$
\begin{aligned}
(l_4')^2 &= (r_P\cos\sigma-r_B)^2+(r_P\sin\gamma\sin\sigma)^2+(-r_P\cos\gamma\sin\sigma+h_2')^2 \\
(l_5')^2 &= \left(-\frac{1}{2}r_P\cos\sigma+\frac{1}{2}r_B\right)^2+\left(-\frac{1}{2}r_P\sin\gamma\sin\sigma+\frac{\sqrt{3}}{2}r_P\cos\gamma-\frac{\sqrt{3}}{2}r_B\right)^2 \\
&\quad+\left(\frac{1}{2}r_P\cos\gamma\sin\sigma+\frac{\sqrt{3}}{2}r_P\sin\gamma+h_2'\right)^2 \\
(l_6')^2 &= \left(-\frac{1}{2}r_P\cos\sigma+\frac{1}{2}r_B\right)^2+\left(-\frac{1}{2}r_P\sin\gamma\sin\sigma-\frac{\sqrt{3}}{2}r_P\cos\gamma+\frac{\sqrt{3}}{2}r_B\right)^2 \\
&\quad+\left(\frac{1}{2}r_P\cos\gamma\sin\sigma-\frac{\sqrt{3}}{2}r_P\sin\gamma+h_2'\right)^2
\end{aligned}
\tag{10}
$$

The position of the *Rod* end P_{RE}' in O_{P2}-$x_{P2}y_{P2}z_{P2}$, i.e. ${}^{P2}P_{RE}'$ can be defined as:

$$
{}^{P2}\boldsymbol{P}_{RE}' = (0,0,l_R)^T \tag{11}
$$

Let x, y, z be the coordinate of ${}^{B1}P_{RE}'$, then end position of the *Rod*, x, y, z in O_{B1}-XYZ can be described as:

$$
\begin{aligned}
(x\quad y\quad z)^T &= {}^{P1}\boldsymbol{R}_1\left({}^{P2}\boldsymbol{R}_2\,{}^{P2}\boldsymbol{P}_{RE}'+{}^{P1}\boldsymbol{O}_{P2}'\right)+{}^{B1}\boldsymbol{O}_{P1}' \\
\therefore\begin{pmatrix}x\\y\\z\end{pmatrix} &= \begin{pmatrix}\cos\beta & 0 & \sin\beta\\ \sin\alpha\sin\beta & \cos\alpha & -\sin\alpha\cos\beta\\ -\cos\alpha\sin\beta & \sin\alpha & \cos\alpha\cos\beta\end{pmatrix}\left[\begin{pmatrix}\cos\sigma & 0 & \sin\sigma\\ \sin\gamma\sin\sigma & \cos\gamma & -\sin\gamma\cos\sigma\\ -\cos\gamma\sin\sigma & \sin\gamma & \cos\gamma\cos\sigma\end{pmatrix}\begin{pmatrix}0\\0\\l_R\end{pmatrix}+\begin{pmatrix}0\\0\\h_2'\end{pmatrix}\right]+\begin{pmatrix}0\\0\\h_1'\end{pmatrix}
\end{aligned}
\tag{12}
$$

3.3 Jacobian matrix

In order to evaluate the motion characteristics of the *Arm*, it is necessary to develop the Jacobian matrix of the *Arm* structure.

As l_i'(i=1,⋯,6), α, β, h_1', γ, σ and h_2' can be taken as functions of time t, noticing $\dot{l}_i'$, $\dot{x}$, $\dot{y}$, $\dot{z}$ are functions of $\dot{\alpha}$, $\dot{\beta}$, $\dot{h}_1'$, $\dot{\gamma}$, $\dot{\sigma}$, $\dot{h}_2'$, the Equation (9), (10), (12) can be differentiated with respect to t, to get the following equations. The ***A***, ***B***, ***C*** are the matrixes with element a_{ij}, b_{ij} (i,j=1,2,3), c_{ij} (i=1,2,3, j=1,⋯, 6), respectively.

$$\begin{pmatrix} \dot{l}_1' \\ \dot{l}_2' \\ \dot{l}_3' \end{pmatrix} = \begin{pmatrix} a_{11} & a_{12} & a_{13} \\ a_{21} & a_{22} & a_{23} \\ a_{31} & a_{32} & a_{33} \end{pmatrix} \begin{pmatrix} \dot{\alpha} \\ \dot{\beta} \\ \dot{h}_1' \end{pmatrix} = \boldsymbol{A} \begin{pmatrix} \dot{\alpha} \\ \dot{\beta} \\ \dot{h}_1' \end{pmatrix}, \qquad \begin{pmatrix} \dot{l}_4' \\ \dot{l}_5' \\ \dot{l}_6' \end{pmatrix} = \begin{pmatrix} b_{11} & b_{12} & b_{13} \\ b_{21} & b_{22} & b_{23} \\ b_{31} & b_{32} & b_{33} \end{pmatrix} \begin{pmatrix} \dot{\gamma} \\ \dot{\sigma} \\ \dot{h}_2' \end{pmatrix} = \boldsymbol{B} \begin{pmatrix} \dot{\gamma} \\ \dot{\sigma} \\ \dot{h}_2' \end{pmatrix}, \tag{13}$$

$$\begin{pmatrix} \dot{x} \\ \dot{y} \\ \dot{z} \end{pmatrix} = \begin{pmatrix} c_{11} & c_{12} & c_{13} & c_{14} & c_{15} & c_{16} \\ c_{21} & c_{22} & c_{23} & c_{24} & c_{25} & c_{26} \\ c_{31} & c_{32} & c_{33} & c_{34} & c_{35} & c_{36} \end{pmatrix} \begin{pmatrix} \dot{\alpha} \\ \dot{\beta} \\ \dot{h}_1' \\ \dot{\gamma} \\ \dot{\sigma} \\ \dot{h}_2' \end{pmatrix} = \boldsymbol{C} \begin{pmatrix} \dot{\alpha} \\ \dot{\beta} \\ \dot{h}_1' \\ \dot{\gamma} \\ \dot{\sigma} \\ \dot{h}_2' \end{pmatrix} \tag{14}$$

Next, the orientation of ${}^{B1}P_{RE}'$ in O_{B1}-XYZ can be expressed by Equation (15), where the element of the matrix ${}^{P1}\boldsymbol{R}_1{}^{P2}\boldsymbol{R}_2$ is presented by r_{ij} (i,j=1,2,3).

$${}^{P1}\boldsymbol{R}_1{}^{P2}\boldsymbol{R}_2 = \begin{pmatrix} cos\beta & 0 & sin\beta \\ sin\alpha sin\beta & cos\alpha & -sin\alpha cos\beta \\ -cos\alpha sin\beta & sin\alpha & cos\alpha cos\beta \end{pmatrix} \begin{pmatrix} cos\sigma & 0 & sin\sigma \\ sin\gamma sin\sigma & cos\gamma & -sin\gamma cos\sigma \\ -cos\gamma sin\sigma & sin\gamma & cos\gamma cos\sigma \end{pmatrix} = \begin{pmatrix} r_{11} & r_{12} & r_{13} \\ r_{21} & r_{22} & r_{23} \\ r_{31} & r_{32} & r_{33} \end{pmatrix} \tag{15}$$

By using Equation (15), the Euler angles (ϕ, θ, ψ) can be acquired (Yoshikawa, 1988).

$$\phi = atan2(r_{23}, r_{13}), \quad \theta = atan2\left(\sqrt{(r_{13})^2 + (r_{23})^2}, r_{33}\right), \quad \psi = atan2(r_{32}, -r_{31}) \quad (0 < \theta < \pi) \tag{16}$$

Equation (17) can be derived by differentiating Equation (16) with regard to time t (Yoshikawa, 1988):

$$\dot{\phi} = \frac{(\dot{r}_{23})r_{13} - r_{23}(\dot{r}_{13})}{(r_{23})^2 + (r_{13})^2}, \quad \dot{\theta} = \frac{\left(\sqrt{(r_{13})^2 + (r_{23})^2}\right)\dot{r}_{33} - \sqrt{(r_{13})^2 + (r_{23})^2}\,(\dot{r}_{33})}{(r_{13})^2 + (r_{23})^2 + (r_{33})^2}, \quad \dot{\psi} = \frac{-(\dot{r}_{32})r_{31} + r_{32}(\dot{r}_{31})}{(r_{32})^2 + (r_{31})^2} \qquad (0 < \theta < \pi) \tag{17}$$

$\dot{\phi}$, $\dot{\theta}$, $\dot{\psi}$ are functions of $\dot{\alpha}$, $\dot{\beta}$, $\dot{\gamma}$, $\dot{\sigma}$. Therefore, by using a matrix D with element d_{ij} (i=1, 2, 3, j=1, 2, 4, 5), $(\dot{\phi}, \dot{\theta}, \dot{\psi})^T$ can be expressed as:

$$\begin{pmatrix} \dot{\phi} \\ \dot{\theta} \\ \dot{\psi} \end{pmatrix} = \begin{pmatrix} d_{11} & d_{12} & 0 & d_{14} & d_{15} & 0 \\ d_{21} & d_{22} & 0 & d_{24} & d_{25} & 0 \\ d_{31} & d_{32} & 0 & d_{34} & d_{35} & 0 \end{pmatrix} \begin{pmatrix} \dot{\alpha} \\ \dot{\beta} \\ \dot{h_1}' \\ \dot{\gamma} \\ \dot{\sigma} \\ \dot{h_2}' \end{pmatrix} = \boldsymbol{D} \begin{pmatrix} \dot{\alpha} \\ \dot{\beta} \\ \dot{h_1}' \\ \dot{\gamma} \\ \dot{\sigma} \\ \dot{h_2}' \end{pmatrix} \tag{18}$$

Equation (14) and (18) can be integrated to the following equation.

$$\begin{pmatrix} \dot{x} \\ \dot{y} \\ \dot{z} \\ \dot{\phi} \\ \dot{\theta} \\ \dot{\psi} \end{pmatrix} = \begin{pmatrix} \boldsymbol{C} \\ \boldsymbol{D} \end{pmatrix} \begin{pmatrix} \dot{\alpha} \\ \dot{\beta} \\ \dot{h_1}' \\ \dot{\gamma} \\ \dot{\sigma} \\ \dot{h_2}' \end{pmatrix} \tag{19}$$

Let inverse matrix of $\boldsymbol{A}$ and $\boldsymbol{B}$ be $\boldsymbol{A}^{-1}$ and $\boldsymbol{B}^{-1}$, which comprise elements $a^{-1}{}_{ij}$, $b^{-1}{}_{ij}$ (i,j=1,2,3), then $\dot{\alpha}, \dot{\beta}, \dot{h_1}', \dot{\gamma}, \dot{\sigma}, \dot{h_2}'$ can be derived from Equation (13).

$$\begin{pmatrix} \dot{\alpha} \\ \dot{\beta} \\ \dot{h_1}' \end{pmatrix} = \boldsymbol{A}^{-1} \begin{pmatrix} \dot{l_1}' \\ \dot{l_2}' \\ \dot{l_3}' \end{pmatrix} = \begin{pmatrix} a^{-1}{}_{11} & a^{-1}{}_{12} & a^{-1}{}_{13} \\ a^{-1}{}_{21} & a^{-1}{}_{22} & a^{-1}{}_{23} \\ a^{-1}{}_{31} & a^{-1}{}_{32} & a^{-1}{}_{33} \end{pmatrix} \begin{pmatrix} \dot{l_1}' \\ \dot{l_2}' \\ \dot{l_3}' \end{pmatrix}, \quad \begin{pmatrix} \dot{\gamma} \\ \dot{\sigma} \\ \dot{h_2}' \end{pmatrix} = \boldsymbol{B}^{-1} \begin{pmatrix} \dot{l_4}' \\ \dot{l_5}' \\ \dot{l_6}' \end{pmatrix} = \begin{pmatrix} b^{-1}{}_{11} & b^{-1}{}_{12} & b^{-1}{}_{13} \\ b^{-1}{}_{21} & b^{-1}{}_{22} & b^{-1}{}_{23} \\ b^{-1}{}_{31} & b^{-1}{}_{32} & b^{-1}{}_{33} \end{pmatrix} \begin{pmatrix} \dot{l_4}' \\ \dot{l_5}' \\ \dot{l_6}' \end{pmatrix}, \quad \therefore \begin{pmatrix} \dot{\alpha} \\ \dot{\beta} \\ \dot{h_1}' \\ \dot{\gamma} \\ \dot{\sigma} \\ \dot{h_2}' \end{pmatrix} = \left(\begin{array}{c|c} \boldsymbol{A}^{-1} & 0 \\ \hline 0 & \boldsymbol{B}^{-1} \end{array}\right) \begin{pmatrix} \dot{l_1}' \\ \dot{l_2}' \\ \dot{l_3}' \\ \dot{l_4}' \\ \dot{l_5}' \\ \dot{l_6}' \end{pmatrix} \tag{20}$$

Therefore, by using Equation (19) and (20), the vector representing the posture of end-effector can be acquired.

$$\begin{pmatrix} \dot{x} \\ \dot{y} \\ \dot{z} \\ \dot{\phi} \\ \dot{\theta} \\ \dot{\psi} \end{pmatrix} = \begin{pmatrix} \boldsymbol{C} \\ \boldsymbol{D} \end{pmatrix} \begin{pmatrix} \dot{\alpha} \\ \dot{\beta} \\ \dot{h_1}' \\ \dot{\gamma} \\ \dot{\sigma} \\ \dot{h_2}' \end{pmatrix} = \begin{pmatrix} \boldsymbol{C} \\ \boldsymbol{D} \end{pmatrix} \left(\begin{array}{c|c} \boldsymbol{A}^{-1} & 0 \\ \hline 0 & \boldsymbol{B}^{-1} \end{array}\right) \begin{pmatrix} \dot{l_1}' \\ \dot{l_2}' \\ \dot{l_3}' \\ \dot{l_4}' \\ \dot{l_5}' \\ \dot{l_6}' \end{pmatrix}$$

$$= \begin{pmatrix} c_{11} & c_{12} & c_{13} & c_{14} & c_{15} & c_{16} \\ c_{21} & c_{22} & c_{23} & c_{24} & c_{25} & c_{26} \\ c_{31} & c_{32} & c_{33} & c_{34} & c_{35} & c_{36} \\ d_{11} & d_{12} & 0 & d_{14} & d_{15} & 0 \\ d_{21} & d_{22} & 0 & d_{24} & d_{25} & 0 \\ d_{31} & d_{32} & 0 & d_{34} & d_{35} & 0 \end{pmatrix} \begin{pmatrix} a^{-1}{}_{11} & a^{-1}{}_{12} & a^{-1}{}_{13} & 0 & 0 & 0 \\ a^{-1}{}_{21} & a^{-1}{}_{22} & a^{-1}{}_{23} & 0 & 0 & 0 \\ a^{-1}{}_{31} & a^{-1}{}_{32} & a^{-1}{}_{33} & 0 & 0 & 0 \\ 0 & 0 & 0 & b^{-1}{}_{11} & b^{-1}{}_{12} & b^{-1}{}_{13} \\ 0 & 0 & 0 & b^{-1}{}_{21} & b^{-1}{}_{22} & b^{-1}{}_{23} \\ 0 & 0 & 0 & b^{-1}{}_{31} & b^{-1}{}_{32} & b^{-1}{}_{33} \end{pmatrix} \begin{pmatrix} \dot{l_1}' \\ \dot{l_2}' \\ \dot{l_3}' \\ \dot{l_4}' \\ \dot{l_5}' \\ \dot{l_6}' \end{pmatrix} = \boldsymbol{J_1} \begin{pmatrix} \dot{l_1}' \\ \dot{l_2}' \\ \dot{l_3}' \\ \dot{l_4}' \\ \dot{l_5}' \\ \dot{l_6}' \end{pmatrix} \tag{21}$$

From the above equation, the Jacobian matrix $\boldsymbol{J}_1$ can be calculated.

3.4 Static mechanics

Let force generated and virtual displacement of each actuator be $\boldsymbol{\tau}$ and $\boldsymbol{\Delta l}$, and the force generated and virtual displacement of *Rod* end P_{RE}' be F and $\boldsymbol{\Delta x}$. From virtual work principle, the relationship between these two pairs is:

$$\boldsymbol{F}^T \boldsymbol{\Delta x} = \tau^T \boldsymbol{\Delta l} \tag{22}$$

By using Equation (21)

$$\boldsymbol{\Delta x} = \boldsymbol{J}_1 \boldsymbol{\Delta l}, \qquad \boldsymbol{J}_1^{-1} \boldsymbol{\Delta x} = \boldsymbol{\Delta l}, \qquad \therefore \boldsymbol{\Delta l} = \boldsymbol{J} \boldsymbol{\Delta x} \ \ (\boldsymbol{J} = \boldsymbol{J}_1^{-1}) \tag{23}$$

Therefore, from Equation (22) and (23), the relation between $\boldsymbol{F}$ and $\boldsymbol{\tau}$ is acquired.

$$\begin{gathered} \boldsymbol{F}^T \boldsymbol{\Delta x} = \tau^T \boldsymbol{J} \boldsymbol{\Delta x}, \qquad \boldsymbol{F}^T = \tau^T \boldsymbol{J}, \qquad \left(\boldsymbol{F}^T\right)^T = \left(\tau^T \boldsymbol{J}\right)^T \\ \therefore \boldsymbol{F} = \boldsymbol{J}^T \tau \end{gathered} \tag{24}$$

4. Method of analysis

In this section, an evaluation index based on the Jacobian Matrix is presented, and the process to evaluate possible configurations, i.e., the physical dimension of the shoulder prosthesis is described.

4.1 An estimative index of manipulability: condition number

The condition number (Arai, 1992) was employed as evaluation indicator for the motion characteristics of the *Arm* mechanism. The condition number is based on the singular value of the Jacobian matrix. The Equation (24) can be described as the expression for how $\boldsymbol{\tau}$ is converted into $\boldsymbol{F}$. Furthermore, a singular value decomposition, expressed by Equation (25), can make the property of $\boldsymbol{J}$ even clearer.

$$\boldsymbol{J}^T = \boldsymbol{U} \boldsymbol{\Sigma} \boldsymbol{V}^T \tag{25}$$

Here, $\boldsymbol{U}$ and $\boldsymbol{V}$ are 6x6 orthogonal matrixes, which can be described by Equation (26).

$$\boldsymbol{U} = \left(\boldsymbol{u}_1, \cdots, \boldsymbol{u}_6\right)^T, \qquad \boldsymbol{V} = \left(\boldsymbol{v}_1, \cdots, \boldsymbol{v}_6\right)^T, \qquad \boldsymbol{\Sigma} = diag(\sigma_1, \cdots, \sigma_6), \ \left(\sigma_1 \geq \sigma_2 \cdots \geq \sigma_6 \geq 0\right) \tag{26}$$

Substituting Equation (25) into (24), the relation between $\boldsymbol{\tau}$ and $\boldsymbol{F}$ can be rewritten as Equation (27).

$$\boldsymbol{F} = \boldsymbol{U} \boldsymbol{\Sigma} \boldsymbol{V}^T \tau, \qquad \boldsymbol{U}^T \boldsymbol{F} = \boldsymbol{\Sigma} \boldsymbol{V}^T \tau \tag{27}$$

Equation (26) and (27) can be rewritten using the elements of $\boldsymbol{U}$ and $\boldsymbol{V}$.

$$\boldsymbol{u}_i^T \boldsymbol{F} = \sigma_i \boldsymbol{v}_i^T \tau \tag{28}$$

Considering the function of the manipulator, it is preferable that the forces that could be generated at the end of the *Rod* in all direction are as uniform as possible. That is, it is the

ratio of the maximum singular value to the minimum one, i.e., the condition number, should be close to 1 as much as possible.

Since the condition number of $\boldsymbol{J}^T$ reflects the both the force and torque working at the end of the *Rod*, in order to conduct proper evaluations, it is necessary to separate the influence of force and torque. Therefore, in the Equation (24), $\boldsymbol{J}^T$ is separated into the part contributing to the force and the one contributing to the torque, and singular value decomposition was conducted at two parts separately. Therefore, $\boldsymbol{J}^T$ is separated as follows.

$$\boldsymbol{J}^T = \begin{bmatrix} \boldsymbol{J}_f{}^T \\ \boldsymbol{J}_m{}^T \end{bmatrix} \tag{29}$$

Here, $\boldsymbol{J}_f{}^T$ and $\boldsymbol{J}_m{}^T$ are 3x6 matrixes, so, three singular values σ_{fi}, σ_{mi}(i=1,2,3) exist in each of $\boldsymbol{J}_f{}^T$ and $\boldsymbol{J}_m{}^T$. Thus, we use the following three condition numbers as estimative index:

$$C = \frac{\sigma_1}{\sigma_6} \tag{31}$$

$$C_f = \frac{\sigma_{f1}}{\sigma_{f3}} \tag{32}$$

$$C_m = \frac{\sigma_{m1}}{\sigma_{m3}} \tag{33}$$

4.2 An outline of the evaluation process

The following is an outline of the evaluation process.

1. Setting up a coordinate space Σ_{CS1};
2. Setting up an initial configuration (physical dimension of the *Arm* mechanism), and modelling the *Arm* and human body in Σ_{CS1};
3. Defining EFAA (Expected Frequently Accessed Area) and RA (Reachable Area) of the *Arm* in Σ_{CS1};
4. For different length of pneumatic actuators, reflecting translational motion of the actuators, numerically calculating and plotting the *Rod* end position P_{RE}';
5. Calculating the estimative indexes for all the P_{RE}' in EFAA and RA;
6. Changing the parameters of the *Arm* mechanism, and going back to recalculating Step 4;
7. After a certain number of loops of execution (Step 4 to 6), evaluating all the configurations to decide configurations optimal for the spatial accessibility (plot number in EFAA) and manipulability.

4.3 Modelling the *Arm* and human body in the coordinate space

A 3D human body model software (HumanWorks) was used for the above-mentioned human body. This HumanWorks model, shown in Fig. 4, 167.0 centimeters tall, is a 50th percentile model of Japanese male based on Japanese Industrial Standards.

Fig. 5(a) shows the coordinate system, $\Sigma_{CS1,}$ for the shoulder prosthetic system. It presents not only the geometry of the *Arm*, and also the EFAA, and their relationship.

As illustrated in the Fig. 5(a), the point of origin is set at the intersection of the median sagittal plane(Y=0), with the horizontal plane(X=0) and the coronal plane(Z=0) passing

through the acrominon. Positions of the acrominon are assumed as (0, ±170, 0). In Fig. 5(c), (d), the size of some parts of human body is presented. Considering the shape and positional relationships of the shoulder, neck, head and the *Arm*, the *Base* 1 of the *Arm* is set at (-80, 150, 0), the axis direction of O_{B1}-XYZ (see Fig. 3) is set to conform to the Z axis of the Σ_{CS1}. Moreover, based on the arm size of the 50th percentile model, we estimated the size of the *Arm* suitable for the human body, and setup initial values for the physical dimension of the *Arm* (Fig. 5(b)). These initial values, which constitute an initial configuration, are summarized as follows (see Fig. 3 for the meanings of the symbols).

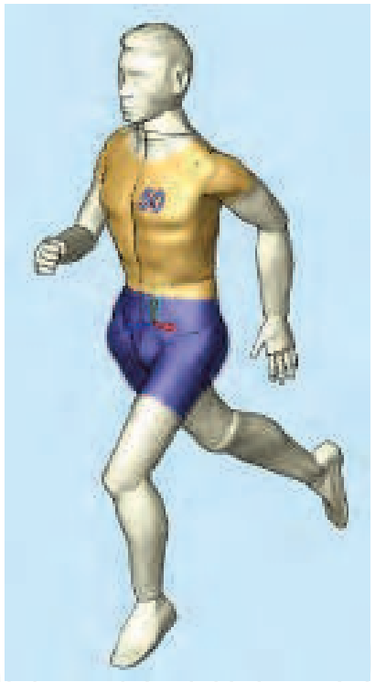

Fig. 4. A 3D human body model of HumanWorks.

$$\begin{aligned} h_1 &= 100 \\ h_2 &= 170 \\ l_R &= 250 \\ r_B &= 50 \\ r_P &= 45 \quad \text{(mm)} \end{aligned} \tag{33}$$

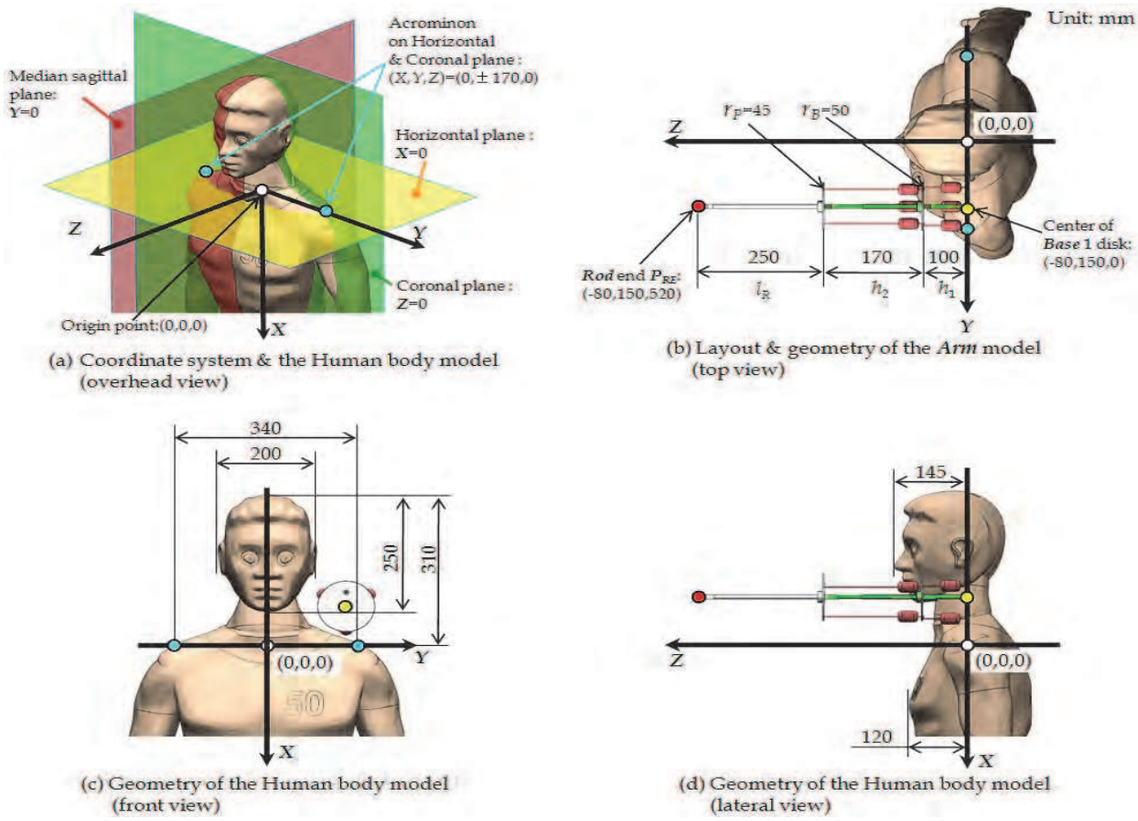

Fig. 5. The coordinate system Σ_{CS1} and the HumanWorks model.

4.4 Important areas in the working space of the *Arm*

Two important areas in the working space of the *Arm* are defined for the analysis and evaluation of the *Arm*. One is the area close to the chest and the median sagittal plane, which is expected to be accessed very frequently during most daily living tasks. This area is the EFAA defined before, and expressed as Σ_{EFAA}. Another is the area that represents the reachable area [RA] of the end effector, defined as Σ_{RA}. Geometries of Σ_{EFAA} and Σ_{RA} are illustrated as in Fig. 6. The volumes of Σ_{EFAA} and Σ_{RA} are set to 12000cm^3 and 75000cm^3, respectively.

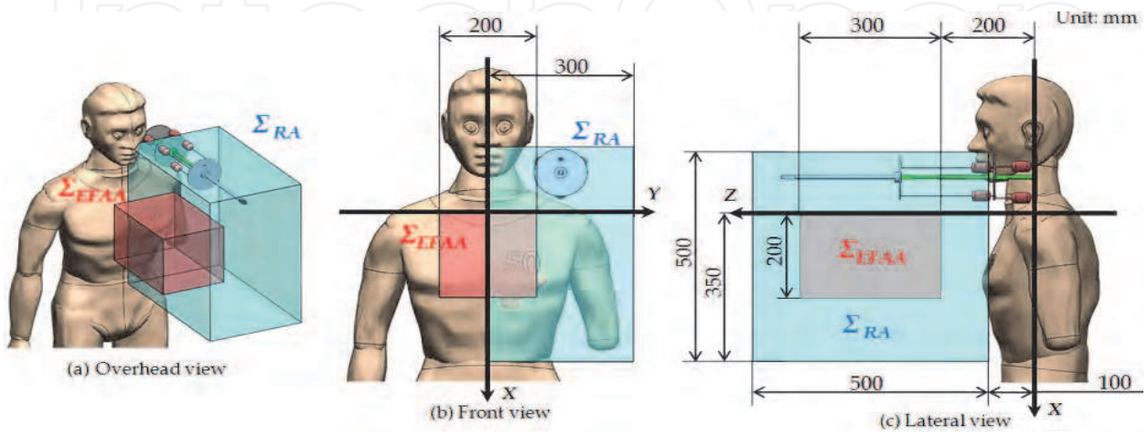

Fig. 6. Geometries of the areas Σ_{EFAA} and Σ_{RA}.

4.5 Calculation and analysis

All the calculation was calculated numerically by using Matlab (MathWorks, Inc.). A simplified *Arm*, as shown in Fig. 7, is drawn for visualization in Matlab. P_{RE}' is calculated by substituting the initial values to Equation (12), with variable length of actuators, which stands for the translational motion of the pneumatic actuators. Three different values were set for each $l_i'(i=1,\cdots,6)$ in Fig. 3(b). Supposing that the resting length of the actuators are LW_i ($i=1,\cdots,6$), and the maximum, minimum, middle increment of the actuators are L_{max}, L_{min}, L_{mid}, then the three different values are $LW_i + L_{max}$, $LW_i + L_{min}$, $LW_i + L_{mid}$ (Fig. 8). Thus, for each *Arm* configuration, a total number of 3^6=729 sets of calculation were calculated for P_{RE}', then the configuration could be evaluated.

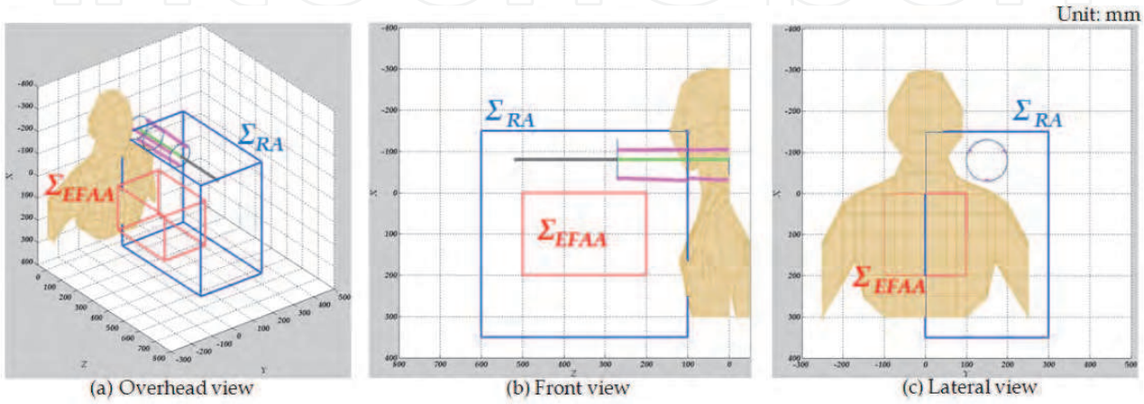

Fig. 7. Models with Matlab.

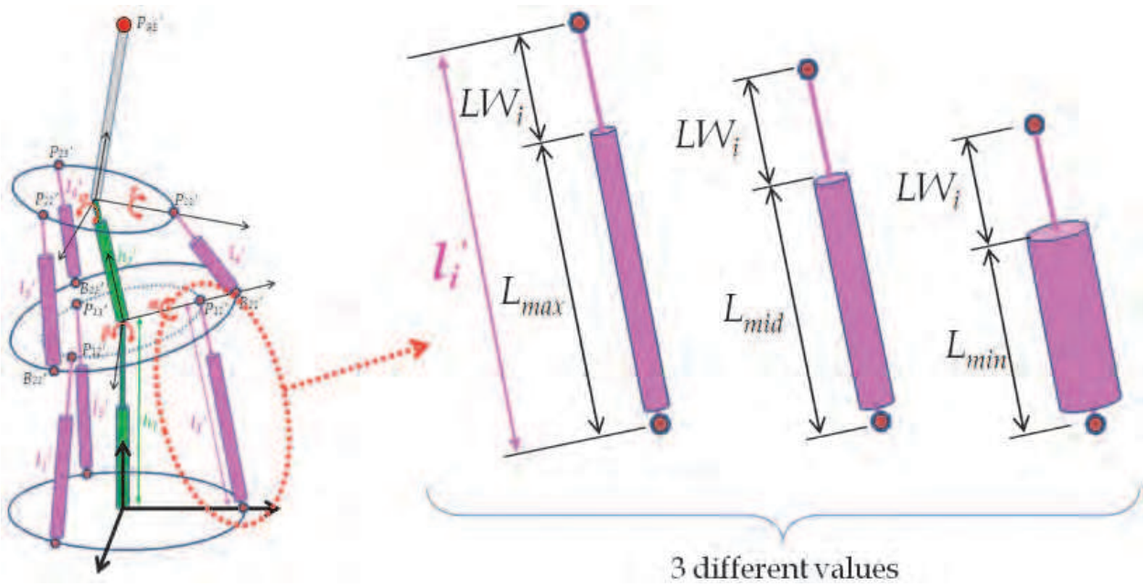

Fig. 8. Three different values of l_i'.

The estimative index described in section 4.1 was adapted as follows, for evaluating different aspects of the system.

- N_{EFAA}: Number of points plotted in Σ_{EFAA} (Spatial accessibility)

- N_{RA}: Number of points plotted in Σ_{RA} (Spatial accessibility)
- $M_t(C)$: 15 percent trimmed mean condition number C (Eq. 30) of points plotted in Σ_{EFAA} (Manipulability)
- $M_t(C_f)$: 15 percent trimmed mean condition number C_f (Eq. 31) of points plotted in Σ_{EFAA} (Manipulability)
- $M_t(C_m)$: 15 percent trimmed mean condition number C_m (Eq. 32) of points plotted in Σ_{EFAA} (Manipulability)

After the calculation and evaluation, the physical dimensions of the *Arm* structure were changed, and the calculation and evaluation for the new configuration were repeated. Note, in this chapter, only the results of changing h_2 and l_R are to be reported.
From this process, optimal configurations of the *Arm* structure could be determined.

5. Results

5.1 Results of the initial configuration

A plot of P_{RE}' for the *Arm* structure with the initial configuration is shown in Fig. 9, where points in red, blue and gray stand for the P_{RE}' located in Σ_{EFAA}, in Σ_{RA} and outside of the both areas, respectively. Basically, the group of points is longitude-axis-symmetric.

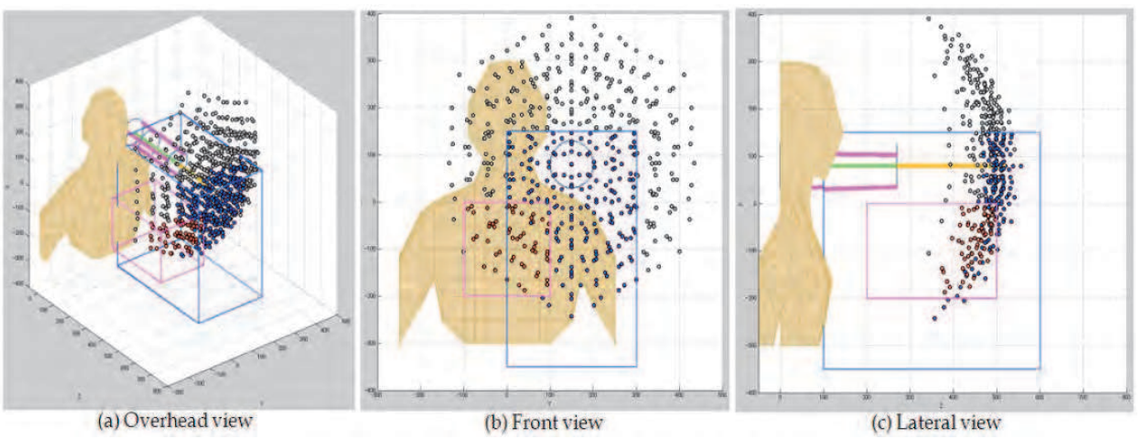

Fig. 9. Plotting P_{RE}' with the initial parameter.

Table 1 shows the values of estimative indexes defined in section 4.5

N_{EFAA}	N_{RA}	$M_t(C)$	$M_t(C_f)$	$M_t(C_m)$
68	393	852240	279.41	1195.5

Table 1. Estimative index with the initial parameter.

5.2 Results of other configurations generated by changing parameters

Suppose that the parameters h_2 and l_R are changed as in Equation (34), where, beginning with 170mm, 250mm (parameters of the initial configuration) h_2 and l_R increase or decrease incrementally by 25mm and 50mm, respectively, and i is an integer, taking value 0, 1, 2.

$$h_2 = 170 \pm 25i$$
$$l_R = 250 \pm 50i \quad (i = 0,1,2) \qquad \text{(mm)} \tag{34}$$

Therefore, a total number of 25 combinations could be made, and identified with No.1-1, ⋯, No.1-25, as shown in Table 2. The estimative indexes were calculated for all the combinations. The N_{EFAA} and N_{RA} are shown in Fig. 10. The horizontal axis stands for the ID of combination, and vertical axis represents N_{EFAA} (Fig. 10(a)) or N_{RA} (Fig. 10(b)).

NO.1-	1	2	3	4	5	6	7	8	9	10	11	12	13
h_2(mm)	120	145	170	195	220	120	145	170	195	220	120	145	170
l_R(mm)	150	150	150	150	150	200	200	200	200	200	250	250	250
NO.1-	14	15	16	17	18	19	20	21	22	23	24	25	
h_2(mm)	195	220	120	145	170	195	220	120	145	170	195	220	
l_R(mm)	250	250	300	300	300	300	300	350	350	350	350	350	

Table 2. Combinations of h_2 and l_R.

Fig. 10(b) shows a tendency that as the *Arm* length l_R gets longer, N_{RA} decreases almost monotonically, but there is a steep descent after No.1-21. This can be attributed to the fact that a certain *Arm* length l_R would make the *Rod* end more likely to go over the Σ_{RA}.

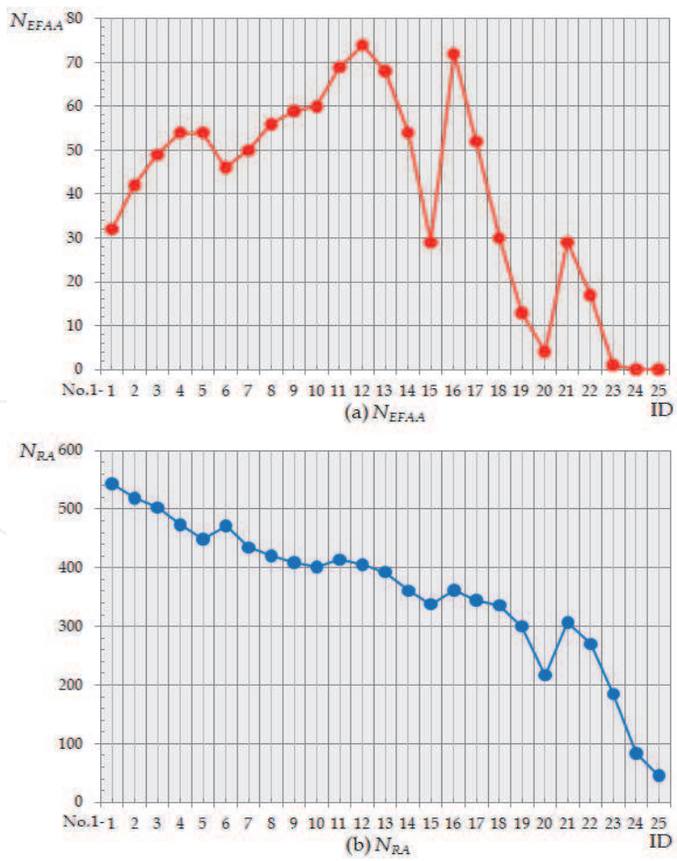

Fig. 10. N_{EFAA} and N_{RA} of 25 combinations of h_2, l_R.

Whereas, as shown in Fig. 10(a), there are roughly two stages. In the stage after No. 1-13, N_{EFAA} decreases while vibrating irregularly and strongly. This can be attributed to the reason same as before: a certain *Arm* length l_R would make the *Rod* end more likely to go over the Σ_{EFAA}. A different point is that the value of No. 1-16, with a smallest h_2 (h_2 = 120mm), shows a large local maximum. It seems h_2 affected N_{EFAA} more than N_{RA}. In the stage before No.1-12, N_{EFAA} gradually increases as the *Arm* length gets longer, which means that it is necessary to precisely investigate the possibility of the *Arm* with shorter length, i.e., smaller l_R and h_2. Thus, the *Arm* with the parameters shown in Equation (35) was investigated.

$$\begin{aligned} h_2 &= 100+7i \\ l_R &= 70+20i \quad (i=0,\cdots,9) \qquad \text{(mm)} \end{aligned} \tag{35}$$

A total number of 100 combinations could be made, and identified with No.2-1, ⋯ , No.2-100, as shown in Table 3. The estimative index was calculated for all the combinations. The results are shown in Table 3 and Fig. 11, 12.

NO.2-	1	2	3	4	5	6	7	8	9	10	11	12	13	14	15	16	17	18	19	20
h_2(mm)	100	107	114	121	128	135	142	149	156	163	100	107	114	121	128	135	142	149	156	163
l_R(mm)	70	70	70	70	70	70	70	70	70	70	90	90	90	90	90	90	90	90	90	90
NO. 2-	21	22	23	24	25	26	27	28	29	30	31	32	33	34	35	36	37	38	39	40
h_2(mm)	100	107	114	121	128	135	142	149	156	163	100	107	114	121	128	135	142	149	156	163
l_R(mm)	110	110	110	110	110	110	110	110	110	110	130	130	130	130	130	130	130	130	130	130
NO. 2-	41	42	43	44	45	46	47	48	49	50	51	52	53	54	55	56	57	58	59	60
h_2(mm)	100	107	114	121	128	135	142	149	156	163	100	107	114	121	128	135	142	149	156	163
l_R(mm)	150	150	150	150	150	150	150	150	150	150	170	170	170	170	170	170	170	170	170	170
NO. 2-	61	62	63	64	65	66	67	68	69	70	71	72	73	74	75	76	77	78	79	80
h_2(mm)	100	107	114	121	128	135	142	149	156	163	100	107	114	121	128	135	142	149	156	163
l_R(mm)	190	190	190	190	190	190	190	190	190	190	210	210	210	210	210	210	210	210	210	210
NO. 2-	81	82	83	84	85	86	87	88	89	90	91	92	93	94	95	96	97	98	99	100
h_2(mm)	100	107	114	121	128	135	142	149	156	163	100	107	114	121	128	135	142	149	156	163
l_R(mm)	230	230	230	230	230	230	230	230	230	230	250	250	250	250	250	250	250	250	250	250

Table 3. Combinations of h_2 and l_R.

As shown in Fig. 11, within the range, as the *Arm* l_R gets longer, N_{EFAA} and N_{RA} changes in the opposite direction: N_{EFAA} increases and N_{RA} decreases. Thus, it is reasonable that, prospective solution for the *Arm* should be specified within this range.

In Fig. 12, the horizontal axis stands for the ID of combination, and vertical axis represents $M_t(C)$ (Fig. 12(a)), $M_t(C_f)$ (Fig. 12(b)) and $M_t(C_m)$ (Fig. 12(c)). There is a steep increase between No. 2-87 and No. 2-88. Since, the smaller value of $M_t(C)$, $M_t(C_f)$ and $M_t(C_m)$ means the better manipulability of the shoulder prosthesis, prospective solutions should be chosen from the combinations before the No. 88.

Apparently, better accessibility requires a bigger value of N_{EFAA} and N_{RA}, however, from the aforementioned results, it is clear that within the range investigated (as shown in Fig. 11), they can not be satisfied simultaneously. That is, N_{EFAA} and N_{RA} should be traded-off depending on which area (EFAA or RA) is more important.

For this purpose, thresholds were determined as follows to reflect different weighting policies and the constraint from manipulability, i.e., $M_t(C)$, $M_t(C_f)$, $M_t(C_m)$. The average μ_0 and standard deviation σ_0 of N_{EFAA}, N_{RA}, $M_t(C)$, $M_t(C_f)$, $M_t(C_m)$ were calculated. For $M_t(C)$, $M_t(C_f)$, $M_t(C_m)$, threshold value was set as $\mu_0+0.5\sigma_0$, which stands for the largest mean value that could be allowed. IN the EFAA-favoured policy, N_{EFAA} should be larger than $\mu_0+0.5\sigma_0$ (upper bound) , but N_{RA} should be at least larger than $\mu_0-0.5\sigma_0$ (lower bound). Similarly, in the RA-favoured policy, N_{RA} should be larger than $\mu_0+0.5\sigma_0$, but, N_{EFAA} should be at least larger than $\mu_0-0.5\sigma_0$. Equation (36)-(a) and (b) show the threshold values reflecting the EFAA-favoured and RA-favoured policies, respectively.

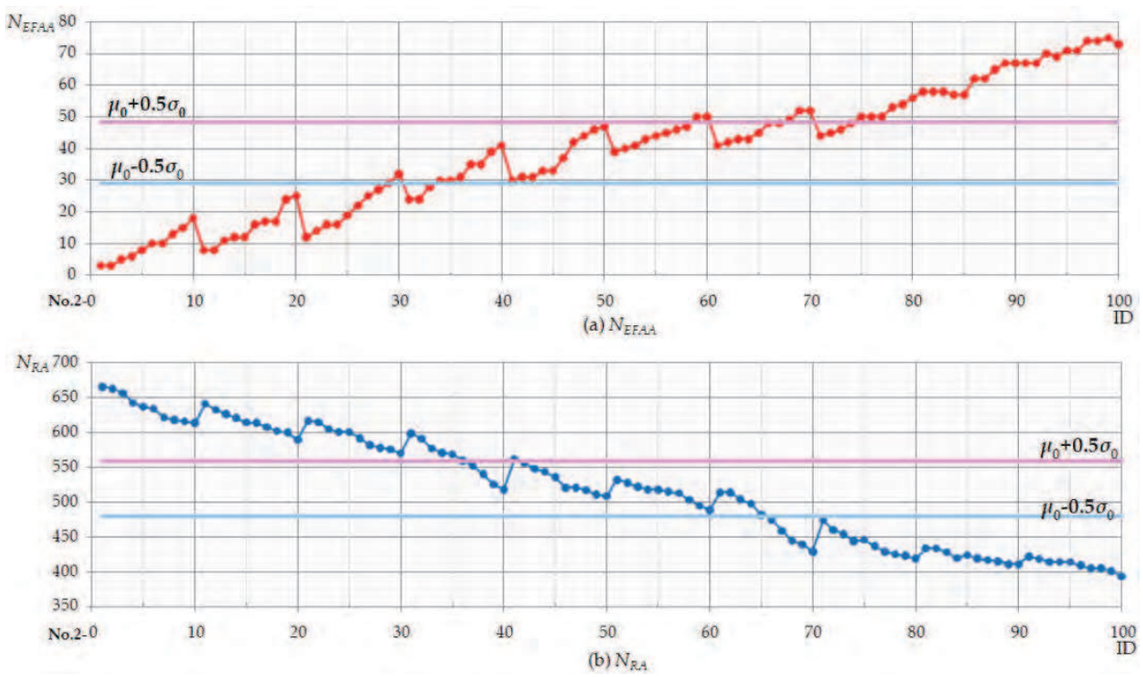

Fig. 11. N_{EFAA} and N_{RA} of 100 combinations of h_2, l_R.

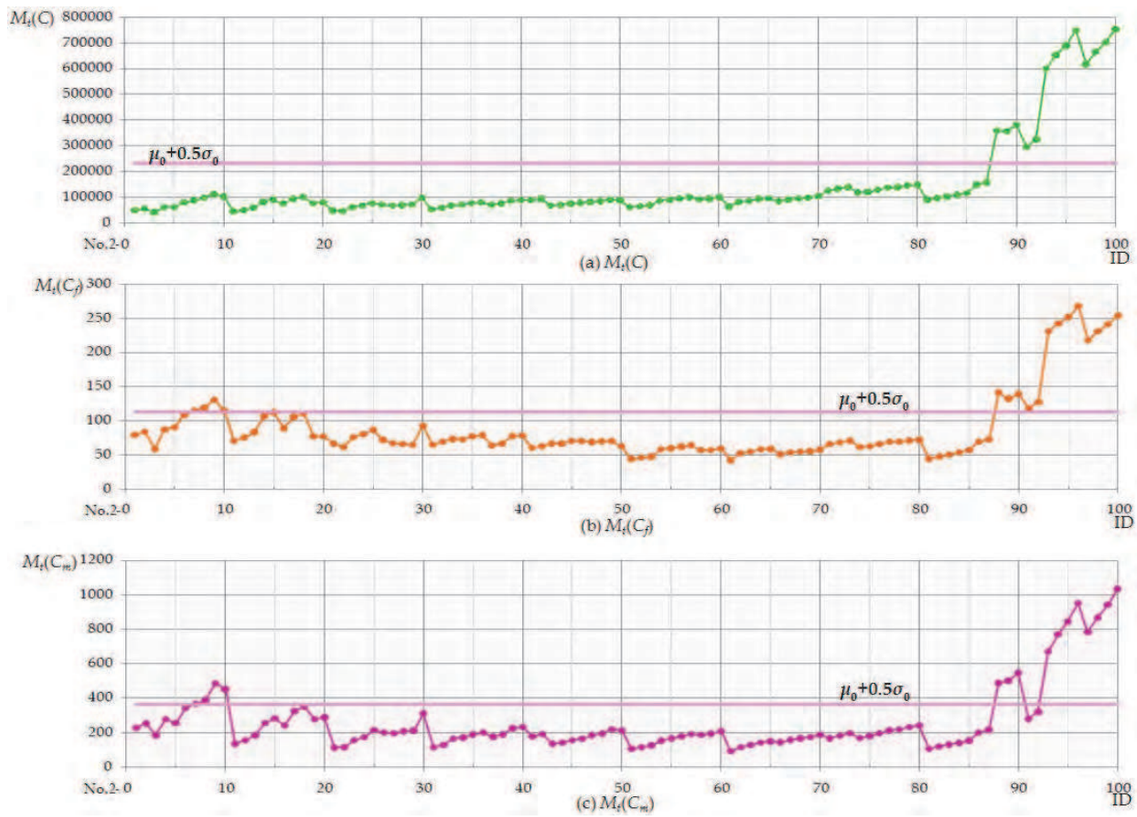

Fig. 12. $M_t(C)$, $M_t(C_f)$ and $M_t(C_m)$ of 100 combinations of h_2, l_R.

$$\left.\begin{array}{l} N_{EFAA} > 48.43 \\ N_{RA} > 480.16 \\ M_t(C) < 232709.74 \\ M_t(C_f) < 113.18 \\ M_t(C_m) < 363.05 \end{array}\right\}\text{(a)} \quad \text{or} \quad \left.\begin{array}{l} N_{EFAA} > 28.97 \\ N_{RA} > 559.78 \\ M_t(C) < 232709.74 \\ M_t(C_f) < 113.18 \\ M_t(C_m) < 363.05 \end{array}\right\}\text{(b)} \tag{36}$$

By using the Equation (36), 8 configuration candidates were selected. In Table 4, the configurations painted red and blue are selected by Equation (36)-(a) and Equation (36)-(b), respectively.

Furthermore, since $M_t(C)$, $M_t(C_f)$, $M_t(C_m)$ are the mean values for C, C_f, C_m, for the configurations selected by the threshold values shown in the Equation (36), there is a possibility that, at some postures, the manipulability might be extremely bad. Therefore, it is necessary to specify the lower bound for the worst manipulability that could be allowed. The following three additional estimative indexes were defined, which means the configuration with a smaller 3rd quartile (the value of a point that divides a data set into 3/4 and 1/4 of points) would be tolerated. They are only defined for EFAA, because this area requires precise manipulation more than RA.

- $Q_3(C)$: the 3rd quartile of C (Eq. 30) of points in Σ_{EFAA}
- $Q_3(C_f)$: the 3rd quartile of C_f (Eq. 31) of points in Σ_{EFAA}
- $Q_3(C_m)$: the 3rd quartile of C_m (Eq. 32)of points in Σ_{EFAA}

NO. 2-	1	2	3	4	5	6	7	8	9	10	11	12	13	14	15	16	17	18	19	20
l_2(mm)	100	107	114	121	128	135	142	149	156	163	100	107	114	121	128	135	142	149	156	163
l_R(mm)	70	70	70	70	70	70	70	70	70	70	90	90	90	90	90	90	90	90	90	90
N_{EFAA}	3	3	5	6	8	10	10	13	15	18	8	8	11	12	12	16	17	17	24	25
N_{RA}	666	663	657	643	637	634	622	618	616	614	641	633	627	621	615	614	608	602	600	590
M_t(C)	50704	56269	41798	61809	62402	80493	87778	98844	112960	103360	45231	50546	60187	82503	90626	75898	93985	101570	77448	80410
M_t(C_f)	79.25	84.21	58.91	87.39	90.53	109.30	114.93	119.21	130.85	114.79	70.65	75.55	83.15	106.78	112.58	89.04	105.86	110.83	77.06	77.25
M_t(C_m)	228.61	253.73	185.23	277.29	255.36	340.25	368.36	387.89	485.79	452.91	136.36	155.24	184.67	256.05	282.46	242.75	325.68	352.09	278.81	289.48
NO. 2-	21	22	23	24	25	26	27	28	29	30	31	32	33	34	35	36	37	38	39	40
l_2(mm)	100	107	114	121	128	135	142	149	156	163	100	107	114	121	128	135	142	149	156	163
l_R(mm)	110	110	110	110	110	110	110	110	110	110	130	130	130	130	130	130	130	130	130	130
N_{EFAA}	12	14	16	16	19	22	25	27	29	32	24	24	28	30	30	31	35	35	39	41
N_{RA}	617	615	605	601	601	592	582	578	576	570	599	591	577	571	569	560	552	540	526	518
M_t(C)	48855	47609	62863	69071	77982	71438	68962	70028	71026	98448	53563	58893	68692	70595	76635	80551	70878	76154	86355	88802
M_t(C_f)	66.87	61.58	76.17	80.51	86.47	72.17	67.07	65.98	64.83	92.55	65.19	69.58	73.46	72.99	77.12	78.90	63.64	66.64	77.58	78.17
M_t(C_m)	113.31	114.71	156.27	173.98	215.79	201.13	196.84	207.91	212.25	311.08	115.32	129.50	164.08	171.75	188.88	201.24	175.38	190.43	225.62	232.43
NO. 2-	41	42	43	44	45	46	47	48	49	50	51	52	53	54	55	56	57	58	59	60
l_2(mm)	100	107	114	121	128	135	142	149	156	163	100	107	114	121	128	135	142	149	156	163
l_R(mm)	150	150	150	150	150	150	150	150	150	150	170	170	170	170	170	170	170	170	170	170
N_{EFAA}	30	31	31	33	33	37	42	44	46	47	39	40	41	43	44	45	46	47	50	50
N_{RA}	562	556	548	544	536	521	521	517	511	509	532	528	522	518	518	515	513	503	495	489
M_t(C)	89754	94852	68424	70380	76201	78502	82345	85105	91295	87927	61794	65769	69759	86706	91159	95923	100940	93368	94581	100830
M_t(C_f)	60.51	62.76	66.86	66.84	70.64	70.61	69.04	69.80	70.50	62.70	44.06	45.93	47.52	58.05	59.97	62.17	64.21	57.00	57.09	59.57
M_t(C_m)	178.42	192.94	134.79	141.66	156.08	164.88	184.89	194.87	218.37	212.98	105.68	115.80	126.23	154.23	166.32	177.94	192.08	188.33	193.69	208.67
NO. 2-	61	62	63	64	65	66	67	68	69	70	71	72	73	74	75	76	77	78	79	80
l_2(mm)	100	107	114	121	128	135	142	149	156	163	100	107	114	121	128	135	142	149	156	163
l_R(mm)	190	190	190	190	190	190	190	190	190	190	210	210	210	210	210	210	210	210	210	210
N_{EFAA}	41	42	43	43	45	48	48	49	52	52	44	45	46	48	50	50	50	53	54	56
N_{RA}	514	514	504	498	482	475	459	445	439	429	474	460	454	444	446	437	429	425	423	419
M_t(C)	64195	82381	87069	93562	96117	85546	91649	95965	97942	104230	126780	133450	140020	117990	121270	129470	137990	139560	145390	149270
M_t(C_f)	42.13	52.51	54.78	58.05	58.98	51.23	53.77	55.19	55.33	57.74	65.96	68.55	71.19	61.53	62.54	65.91	69.30	69.33	71.23	72.07
M_t(C_m)	92.34	116.28	128.30	141.54	149.27	144.18	157.25	167.21	174.10	187.66	167.59	183.12	197.12	170.24	180.53	196.54	213.14	219.68	231.90	241.78
NO. 2-	81	82	83	84	85	86	87	88	89	90	91	92	93	94	95	96	97	98	99	100
l_2(mm)	100	107	114	121	128	135	142	149	156	163	100	107	114	121	128	135	142	149	156	163
l_R(mm)	230	230	230	230	230	230	230	230	230	230	250	250	250	250	250	250	250	250	250	250
N_{EFAA}	58	58	58	57	57	62	62	65	67	67	67	67	70	69	71	71	74	74	75	73
N_{RA}	434	434	428	420	424	419	417	415	411	411	422	418	414	414	414	409	405	405	401	393
M_t(C)	90894	97221	103940	109450	116780	149070	158490	359530	357440	381760	296780	325030	600120	654050	690430	749300	617550	665350	703810	753910
M_t(C_f)	44.48	47.42	50.40	54.04	57.11	69.18	72.59	141.36	132.40	139.36	118.09	127.62	231.17	242.59	251.72	268.34	218.07	231.35	241.08	254.22
M_t(C_m)	107.26	118.82	131.14	139.62	152.66	199.98	216.74	487.80	502.54	546.75	280.27	321.11	672.03	770.05	845.97	951.96	783.71	868.60	942.70	1034.10

Table 4. Combinations of h_2 and l_R.

Fig. 13 shows the values of the new estimative indexes $Q_3(C)$, $Q_3(C_f)$ and $Q_3(C_m)$ for 100 configurations listed in Table 4. $Q_3(C_m)$ oscillated with a gradually decreasing peak-to-peak value. $Q_3(C)$, $Q_3(C_f)$ oscillated, with a biggest peak-to-peak value of 20000, and 250 respectively, and turned to stable at a comparatively low level between No.2-50 to No.2-70. Thus it is clear that these new indexes could provide useful information to select optimal *Arm* configurations further.

The values of all the estimative indexes for the selected configurations (for both EFAA-favoured and RA-favoured policies) are shown in Table 5, and Fig. 14.

NO. 2-	29	30	34	35	36	41	59	60
h_2(mm)	156	163	121	128	135	100	156	163
l_R(mm)	110	110	130	130	130	150	170	170
N_{EFAA}	29	32	30	30	31	30	50	50
N_{RA}	576	570	571	569	560	562	495	489
M_t(C)	71026	98448	70595	76635	80551	89754	94581	100830
M_t(C_f)	64.83	92.55	72.99	77.12	78.90	60.51	57.09	59.57
M_t(C_m)	212.25	311.08	171.75	188.88	201.24	178.42	193.69	208.67
Q_3(C)	83723	185210	183300	201290	183480	148600	105920	112380
Q_3(C_f)	32.50	163.16	213.12	226.05	186.47	175.16	32.28	33.70
Q_3(C_m)	309.56	498.23	332.77	371.69	365.79	229.55	338.79	365.39

Table 5. 8 values of the estimative indexes for selected configurations.

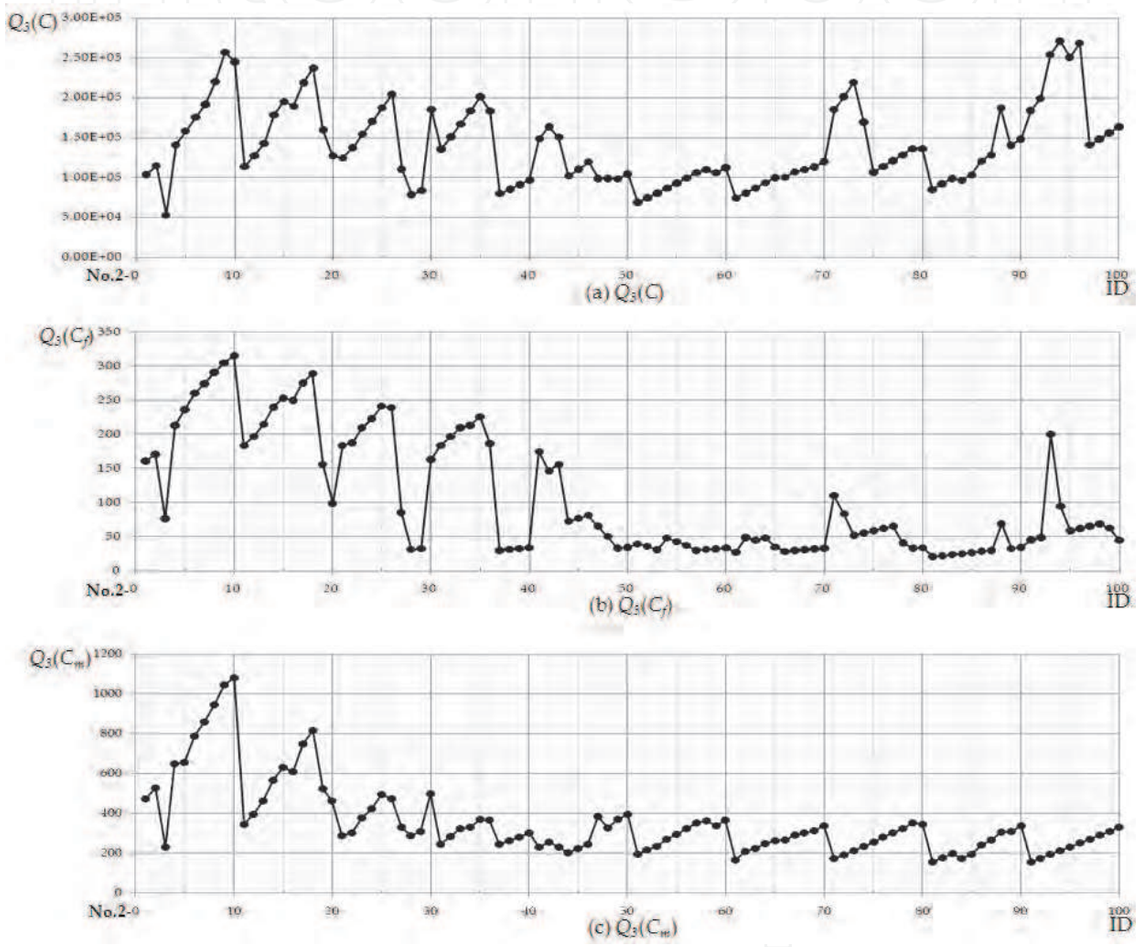

Fig. 13. $Q_3(C)$, $Q_3(C_f)$ and $Q_3(C_m)$ of 100 configurations listed in Table 4.

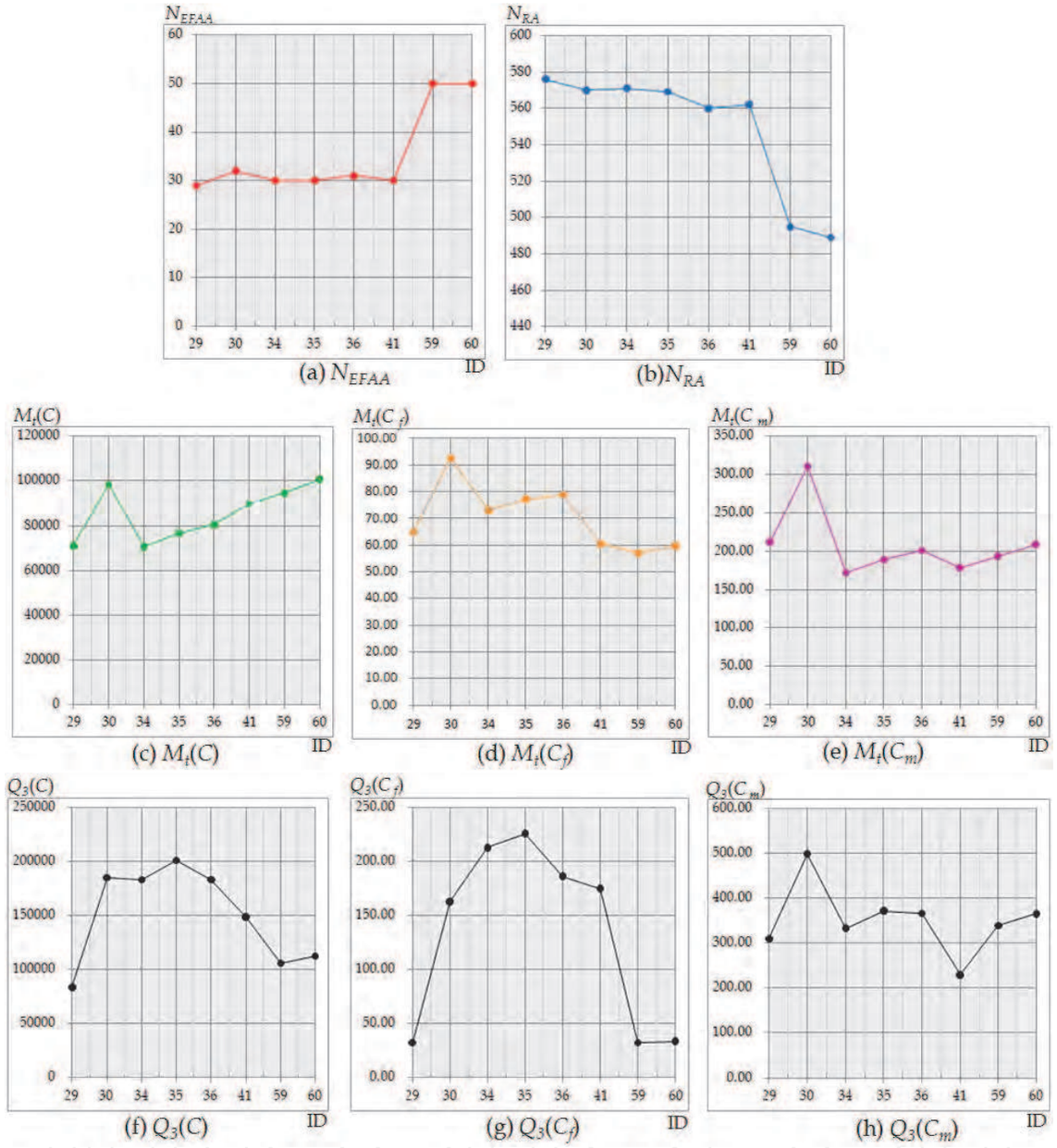

Fig. 14. Plots of values of the estimative indexes of 8 selected configurations.

It is certain that the selected configuration No.2-29, 30, 34, 35, 36, 41 resulted in a larger N_{RA}, and configuration No.2-59, 60 made a larger N_{EFAA}. Considering the N_{RA}, N_{EFAA} and $Q_3(C)$, $Q_3(C_f)$, $Q_3(C_m)$ together, among the RA-favoured configuration, No.2-29, among the EFAA-favoured, No.2-59 are the optimal configurations.

6. Discussion

Optimal configurations were selected, using the estimative indexes proposed. How the selected configurations meet the requirements of the shoulder prostheses for daily living is

the most important concern. Prototyping and experiments in real daily living environment are necessary to give the evaluation. However, on this research stage, preliminary verification could be done by comparing one selected configuration with the initial solution. The comparison was shown in Table 6 and Fig. 15.

Index	h_2-l_R Combination		Upgrading (%)
	Initial	Optimal(No.2-59)	
h_2(mm)	170	156	
l_R(mm)	250	170	
N_{EFAA}	68	50	-26.47
N_{RA}	393	495	25.95
$M_t(C)$	852240	94581	88.90
$M_t(C_f)$	279.41	57.09	79.57
$M_t(C_m)$	1195.50	193.69	83.80
$Q_3(C)$	160460	105920	33.99
$Q_3(C_f)$	57.51	32.28	43.87
$Q_3(C_m)$	324.22	338.79	-4.49

Table 6. A comparison between the optimal with the initial configuration.

As shown in Table 6, all the other indexes are improved at a price of 26.47% reduce of N_{EFAA}. This could be improved or compensated by 1) including h_1, and disk size r_B, r_P, as design parameters to enable better combinations; 2) employing a flexible backbone; 3) increasing actuators' operating range by changing pneumatic actuators, or serially connecting the current actuators.

There is another important clue shown in Fig. 15. There are 2 relative features of the selected configuration: 1) plots of the selected configuration are more compact than the initial solution; 2) the center of the plot distribution locates quite far from the center of the EFAA. Due to the two features, there are fewer points plotted in Σ_{EFAA}. However, if the center of this compact distribution could be directed towards the center of EFAA, much better configuration could be expected. The relocation of the distribution center could be realized by biasing the initial posture of the shoulder prosthesis, i.e., adjusting resting length of actuators.

Considering the fact that the *Arm* is used as shoulder prostheses, twisting or bending users' trunk could also contribute to the posture control. However, this is not preferable, since it could result in fatigue damage accumulation in lower back muscles, due to frequent use of upper limb in daily living. That is why the spatial accessibility would be a very important issue in our future research. Moreover, the existence of singular points should be confirmed, and investigation from the viewpoint of mechanics should be done.

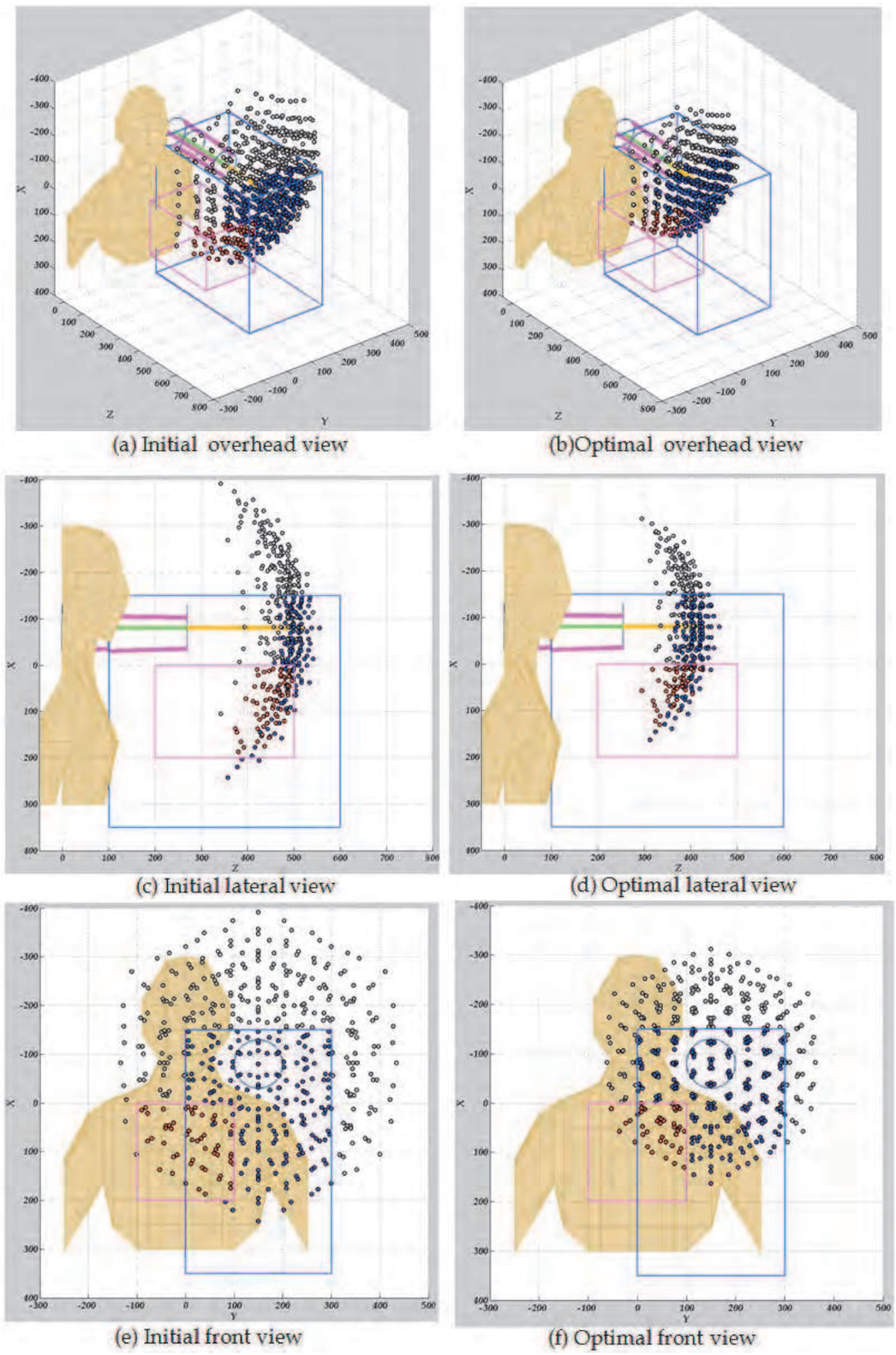

Fig. 15. A comparison between the optimal with the initial configuration.

7. Conclusion

In the research, approach to optimize configuration for shoulder prostheses considering the spatial accessibility and manipulability was proposed. Since for an individual user, the preferable EFAA and RA might be different due to individual difference in daily living style and tasks, and physical constitution, rather than configuration itself, the approach to find the configuration is more important. Thus our research could facilitate the design process of shoulder prostheses with constrained functional elements.
In the near future, estimative indexes to evaluate spatial distribution should be devised, with which the items for further investigation mentioned in the section 6 should be carried out and verified.

8. Acknowledgment

This work was supported in part by a Grant-in-Aid for Scientific Research (B), 2011, 23300206, from the Ministry of Education, Culture, Sports, Science and Technology of Japan, and by the Mitsubishi Foundation.

9. References

Airic's_arm. (2000-2008). March 23, 2011, Available from: <http://www.festo.com/cms/en-us_us/5009.htm>, Festo AG & Co. KG

Arai, T. (1992). Analysis and Synthesis of a Parallel Link Manipulator Based on Its Statics, *Journal of the Robotics Society of Japan*, Vol. 10, No. 4, pp.526–533 (in Japanese).

Folgheraiter, M. & Gini, G. (2005). MaximumOne: An Anthropomorphic Arm with Bio-inspired Control System, *Biomimetic Neural Learning for intelligent robots*, LNAI 3575, pp. 281–298, ISBN 978-3-540-27440-7

Jacobson, S. C.; Knutti, D. F.; Johnson, R. T. & Sears, H. H. (1982). Development of the Utah Artificial Arm, *IEEE Transactions on Biomedical Engineering*, Vol. 29, No. 4, pp. 249-269, April

Ku, D. M. (1999). Direct displacement analysis of a Stewart platform mechanism, *Mechanism and Machine Theory*, 34, pp. 453-465.

Merlet, J. P. (1993). Direct kinematics of parallel manipulators, *IEEE Transactions on Robotics and Automation*, Vol. 9, No. 6, pp. 842-846, December

Nasu, M.; Ohnishi, K.; Tajima, T. & Saito, Y. (2001). Study on Hybrid Electric Prosthesis for Single Arm Amputee, *Proceedings of the 7th Conference on Japan Society of Mechanical Engineers Kanto Branch*, Vol. 7, pp.133-134, March 9, 2001, Japan (in Japanese)

Press, W. H.; Teukolsky, S. A.; Vetterling, W. T. & Flannery, B. P. (1992). *Numerical Recipes in C The Art of Scientific Computing Second Edition*, pp. 379-383, Cambridge University Press

Revolutionizing Prosthetics 2009. (2011). March 23, 2011, Available from: <http://www.jhuapl.edu/ourwork/stories/st090829.asp>,The Johns Hopkins University Applied Physics Laboratory

The investigation of disabled person and child. (2005). March 23, 2011, Available from: <http://www.mhlw.go.jp/toukei/list/108-1.html>, Ministry of Health, Labour and Welfare (in Japanese)

Troncossi, M.; Borghi, C.; Chiossi, M.; Davalli, A. & Parenti-Castelli, V. (2009a). Development of a prosthesis shoulder mechanism for upper limb amputees: application of an original design methodology to optimize functionality and

wearability, *Medical and Biological Engineering and Computing*, Vol. 47, No. 5, pp.523-531

Troncossi, M.; Gruppioni, E.; Chiossi, M.; Cutti, A. G.; Davalli, A. & Parenti-Castelli, V. (2009b). A Novel Electromechanical Shoulder Articulation for Upper-Limb Prostheses: From the Design to the First Clinical Application, *JPO Journal of Prosthetics and Orthotics*, Vol. 21, Issue 2, pp. 79-90, April 2009,

Troncossi, M.; Parenti-Castelli, V. & Davalli, A. (2005). Mechanical design of a prosthetic shoulder mechanism for upper limb amputees, *Proceedings of the 2005 IEEE 9th International Conference on Rehabilitation Robotics*, June 28 - July 1, 2005, Chicago, IL, USA

Utah Arm 3. (2006-2011). March 23, 2011, Available from: <http://www.utaharm.com/ua3.php>, Motion Control, Inc.

Yoshikawa, T. (1988). *Foundations of Robot Control*, Corona Publishing Co., Ltd., ISBN 978-4-339-04130-9 (in Japanese)

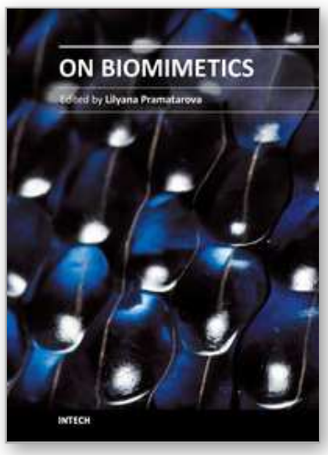

On Biomimetics

Edited by Dr. Lilyana Pramatarova

ISBN 978-953-307-271-5
Hard cover, 642 pages
Publisher InTech
Published online 29, August, 2011
Published in print edition August, 2011

Bio-mimicry is fundamental idea â€˜How to mimic the Natureâ€™ by various methodologies as well as new ideas or suggestions on the creation of novel materials and functions. This book comprises seven sections on various perspectives of bio-mimicry in our life; Section 1 gives an overview of modeling of biomimetic materials; Section 2 presents a processing and design of biomaterials; Section 3 presents various aspects of design and application of biomimetic polymers and composites are discussed; Section 4 presents a general characterization of biomaterials; Section 5 proposes new examples for biomimetic systems; Section 6 summarizes chapters, concerning cells behavior through mimicry; Section 7 presents various applications of biomimetic materials are presented. Aimed at physicists, chemists and biologists interested in biomineralization, biochemistry, kinetics, solution chemistry. This book is also relevant to engineers and doctors interested in research and construction of biomimetic systems.

How to reference

In order to correctly reference this scholarly work, feel free to copy and paste the following:

Masashi Sekine, Kento Sugimori and Wenwei Yu (2011). To Design a Small Pneumatic Actuator Driven Parallel Link Mechanism for Shoulder Prostheses for Daily Living Use, On Biomimetics, Dr. Lilyana Pramatarova (Ed.), ISBN: 978-953-307-271-5, InTech, Available from: http://www.intechopen.com/books/on-biomimetics/to-design-a-small-pneumatic-actuator-driven-parallel-link-mechanism-for-shoulder-prostheses-for-dail

INTECH
open science | open minds

InTech Europe
University Campus STeP Ri
Slavka Krautzeka 83/A
51000 Rijeka, Croatia
Phone: +385 (51) 770 447
Fax: +385 (51) 686 166
www.intechopen.com

InTech China
Unit 405, Office Block, Hotel Equatorial Shanghai
No.65, Yan An Road (West), Shanghai, 200040, China
中国上海市延安西路65号上海国际贵都大饭店办公楼405单元
Phone: +86-21-62489820
Fax: +86-21-62489821

© 2011 The Author(s). Licensee IntechOpen. This chapter is distributed under the terms of the Creative Commons Attribution-NonCommercial-ShareAlike-3.0 License, which permits use, distribution and reproduction for non-commercial purposes, provided the original is properly cited and derivative works building on this content are distributed under the same license.

IntechOpen

IntechOpen